The ubiquitin-proteasome system functionally links neuronal Tomosyn-1 to dendritic morphology

Received for publication, August 31, 2017, and in revised form, December 2, 2017 Published, Papers in Press, December 21, 2017, DOI 10.1074/jbc.M117.815514

Johnny J. Saldate[‡], Jason Shiau[§], Victor A. Cazares[§], and Edward L. Stuenkel[‡§1]

From the [‡]Neuroscience Graduate Program and the [§]Department of Molecular and Integrative Physiology, Medical School, University of Michigan, Ann Arbor, Michigan 48109-5624

Edited by F. Anne Stephenson

Altering the expression of Tomosyn-1 (Tomo-1), a soluble, R-SNARE domain–containing protein, significantly affects behavior in mice, *Drosophila*, and *Caenorhabditis elegans*. Yet, the mechanisms that modulate Tomo-1 expression and its regulatory activity remain poorly defined. Here, we found that Tomo-1 expression levels influence postsynaptic spine density. Tomo-1 overexpression increased dendritic spine density, whereas Tomo-1 knockdown (KD) decreased spine density. These findings identified a novel action of Tomo-1 on dendritic spines, which is unique because it occurs independently of Tomo-1's C-terminal R-SNARE domain. We also demonstrated that the ubiquitin-proteasome system (UPS), which is known to influence synaptic strength, dynamically regulates Tomo-1 protein levels. Immunoprecipitated and affinity-purified Tomo-1 from cultured rat hippocampal neurons was ubiquitinated, and the levels of ubiquitinated Tomo-1 dramatically increased upon pharmacological proteasome blockade. Moreover, Tomo-1 ubiquitination appeared to be mediated through an interaction with the E3 ubiquitin ligase HRD1, as immunoprecipitation of Tomo-1 from neurons co-precipitated HRD1, and this interaction increases upon proteasome inhibition. Further, *in vitro* reactions indicated direct, HRD1 concentration–dependent Tomo-1 ubiquitination. We also noted that the UPS regulates both Tomo-1 expression and functional output, as HRD1 KD in hippocampal neurons increased Tomo-1 protein level and dendritic spine density. Notably, the effect of HRD1 KD on spine density was mitigated by additional KD of Tomo-1, indicating a direct HRD1/Tomo-1 effector relationship. In summary, our results indicate that the UPS is likely to participate in tuning synaptic efficacy and spine dynamics by precise regulation of neuronal Tomo-1 levels.

Synaptic structure and activity within the central nervous system are continually modified as the result of ongoing cognitive, affective, motor, and environmental experiences. Manifestations of this plasticity, although diverse in mechanism, are largely composed of dynamic changes in the molecular regulation of synaptic efficacy, intrinsic electrical properties, and/or cell morphology. Although activity-dependent regulation of the synaptic proteome via *de novo* translation has long been recognized (1, 2), it was not until the 1990s that the role of the ubiquitin-proteasome system (UPS)[2] began to be appreciated in targeted degradation of proteins participating in synaptic plasticity (3).

Accumulating evidence has now established a key role for the UPS in regulating the development and efficacy of synapses (4–6). Acting within both presynaptic and postsynaptic compartments, the UPS has been reported to control a number of specific actions, including synapse maturation and maintenance, silencing presynaptic activity, and inhibiting the assembly of SNARE core complexes (7–10). The UPS also determines the AMPA receptor content and functional state of the postsynaptic density (PSD) (11, 12), degrading scaffolding proteins and neurotransmitter receptors, in response to neural activity directing proteasomes to dendritic spines (13, 14). Moreover, extensive evidence implicates the UPS in regulating spine dynamics (15) and trans-synaptic plasticity (16). Differential targeting of positive and negative regulators of synaptic plasticity by the UPS is therefore proposed to contribute to the physiological dynamic range of neurotransmitter release and reception and, hence, the efficacy of information transfer at synapses.

Tomosyn-1 (Tomo-1) is a soluble, SNARE-family protein, primarily known as a potent negative regulator of vesicle fusion (17) that strongly reduces evoked exocytosis of neurotransmitter-containing vesicles (18–20) and plasticity induction within the brain (21–23). Although soluble, Tomo-1 also associates with secretory vesicles and plasma membranes in neuroendocrine cells (24, 25) and neurons (26–28). Tomo-1 has been observed to regulate neurite outgrowth and increase branching complexity in developing cultured rat hippocampal neurons and chemically differentiated NG108 cells (29). Moreover, our recent study demonstrated an importance of Tomo-1 in modulating distribution of presynaptic vesicles among functionally defined vesicle pools, separating actively recycling vesicles from non-fusogenic resting vesicles (30).

This work was supported by National Institutes of Health Grant R01 NS097498 (to E. L. S.). Additional training support was provided by National Institutes of Health Grant F31 NS087883 (to J. J. S.). The authors declare that they have no conflicts of interest with the contents of this article. The content is solely the responsibility of the authors and does not necessarily represent the official views of the National Institutes of Health.

[1] To whom correspondence should be addressed. Tel.: 734-763-4477; Fax: 734-647-0717; E-mail: esterm@umich.edu.

[2] The abbreviations used are: UPS, ubiquitin-proteasome system; Tomo-1, Tomosyn-1; ASD, autism spectrum disorder; IP, immunoprecipitation; PLA, proximity ligation assay; DIV, days *in vitro*; KD, knockdown; SCR, scrambled control; ΔCT, C-terminal deletion; ANOVA, analysis of variance; co-IP, co-immunoprecipitation; CDK5, cyclin-dependent kinase 5; ICC, immunocytochemistry; LSCM, laser-scanning confocal microscopy; ER, endoplasmic reticulum; 2KD, double KD condition; RRP, readily releasable pool; PTM, post-translational modification; CNQX, 7-nitro-2,3-dioxo-1,4-dihydroquinoxaline-6-carbonitrile; NA, numerical aperture.

Highly conserved orthologs of Tomo-1 are found in *Saccharomyces cerevisiae* (Sro7p/77p), *Caenorhabditis elegans* (TOM-1), and *Drosophila melanogaster* (Lgl), where they appear to exhibit strong similarities in structural properties (31–35) and mechanistic actions (36–38). TOM-1 has been reported to participate in trans-synaptic plasticity via the neurexin–neuroligin pathway in *C. elegans* (39). Tomo-1 is also critical for some forms of plasticity and memory, including hippocampal-dependent learning and memory in mice (22), and associative odor memory in *D. melanogaster* (21). These reports suggest the activity and functional impacts of Tomo-1 may be dynamically modifiable as a result of neural activity.

Tomo-1 is subject to multiple forms of post-translational modification in neurons, including phosphorylation by PKA (36) and CDK5 (30), and SUMOylation (40) by PIASγ (41). Although PKA phosphorylation at serine-724 and SUMOylation at lysine-730 both reduce the inhibitory actions of Tomo-1, they do so by different means, as only PKA phosphorylation reduces Tomo-1 interaction with the R-SNARE syntaxin-1a. By comparison, CDK5 phosphorylation of Tomo-1 has been reported to increase its inhibitory properties on membrane trafficking (30). Sro7p/77p also functionally regulate membrane vesicle trafficking with their activity subject to regulation by Rab-GTPases (Sec4) and a type V myosin (Myo2) (31). Like Tomo-1, the related Tomo-2 protein is also expressed within cytoplasm of neurons, including those within the hippocampus in mice (42). Interestingly, expression of Tomo-2 in HEK293T or the insulin-secreting INS1 cell lines revealed it was a target of UPS-mediated degradation (43). However, the role of the UPS in regulating Tomo-1 level within neurons remains unknown.

Characterizing processes determining Tomo-1 protein level and functional state is important based on Tomo-1's key role in modulating vesicle release probability and trans-synaptic tuning in neurons. The purpose of the current study was to examine UPS-mediated regulation of Tomo-1 in hippocampal neurons and the impact of this regulation on synaptic structure. In addition, SNARE-domain containing proteins, including Tomo-1, and the UPS have been linked to the proteinopathy and protein aggregation associated with neurological and neurodegenerative diseases, including autism spectrum disorders (ASD) (44–46), Alzheimer's disease (AD) (47, 48), and Parkinson's disease (PD) (49, 50). Specifically, Tomo-1 gene variation in humans has been correlated with ASD (51).

Results

Tomo-1 expression level alters dendritic spine density

Because Tomo-1 is reported to alter membrane trafficking and vesicle fusion, we initially examined whether Tomo-1 alters the density or morphology of dendritic spines in synaptically mature cultures of rat hippocampal neurons (17–24 days *in vitro* (DIV)). Neurons were transfected with a soluble mCherry fluorophore and co-transfected with one of the following expression constructs: 1) N-terminal–tagged eGFP m–Tomo-1 (Tomo-1), 2) eGFP m–Tomo-1 containing a C-terminal R-SNARE motif deletion (ΔCT), 3) cytosolic eGFP, as a control for the overexpression of vectors containing eGFP, 4) shRNA targeting m–Tomo-1 for knockdown (KD), and 5) the same shRNA vector with a scrambled nucleotide sequence replacing the Tomo-1 target sequence. In addition, we examined a condition in which shRNA KD of rat Tomo-1 was rescued with co-transfection of shRNA-resistant human N-terminal–tagged mCherry–Tomo-1. Effectiveness of the Tomo-1 KD and rescue was confirmed by both immunocytochemistry (ICC) (Fig. 1*A*, *B* and *D*) and Western blot analysis (Fig. 1, *C* and *D*). ICC was quantified in transfected, shRNA-expressing neurons, relative to neighboring nontransfected control neurons. High-resolution confocal imaging of neurons transfected with GFP Tomo-1 also demonstrated localization within the cytosol to dendrites and spines (Fig. 1*E*). For spine analysis co-expression of mCherry and either GFP Tomo-1 or shRNA constructs also encoding GFP was confirmed by imaging of both mCherry and GFP spectral lines. Western blotting of lysates from virally infected neuronal cultures demonstrated that our expression constructs successfully knock down, overexpress, and rescue Tomo-1 in neurons (Fig. 1, *C* and *D*). To restrict fluorescence analysis to processes arising from individual neurons, we transfected cultures under conditions generating low transfection efficiency (~2–5 cells per coverslip). To assess alterations in dendritic spine density and morphology, transfected neurons were subjected to laser-scanning confocal microscopy (LSCM) of mCherry fluorescence intensity over a series of Z-planes. Acquired Z-stacks were subsequently compiled to render 3D reconstructed dendrites from which spine density and morphology was quantified by following a single dendritic arbor projecting from each neuronal cell body. Representative images of dendrite segments for each condition tested are shown in Fig. 1*F*.

Importantly, our results demonstrate that exogenous Tomo-1 expression specifically and significantly increased average spine density. In contrast, shRNA-mediated KD decreased dendritic spine density, an effect overcome by Tomo-1 rescue, relative to respective controls (Fig. 1*G*). This identifies a novel postsynaptic function for Tomo-1, as the sparse transfection makes an indirect presynaptic effect unlikely. Notably, this effect occurred independently of Tomo-1's C-terminal R-SNARE domain. That is, the effects on spine density of Tomo-1 lacking its R-SNARE domain (ΔCT) were not significantly different from those overexpressing wildtype Tomo-1. Expression of the scrambled shRNA control sequence (SCR) had no significant effect on spine density relative to GFP control. Although Tomo-1 overexpression and knockdown was found to affect spine density, no significant effects were found on total spine length (Fig. 1*H*), spine head maximum diameter (Fig. 1*I*), or spine head volume (Fig. 1*J*). However, the rescue of Tomo-1 expression did indicate increases in maximum spine head diameter and volume (Fig. 1, *I* and *J*, *purple*). Moreover, as shown in Fig. 1, *K* and *L*, cumulative frequency distributions of dendrite spine count *versus* distance from neuronal soma confirmed statistically significant differences between Tomo-1, ΔCT, and KD relative to respective controls. Notably, the cumulative distributions were generally linear for each condition, indicating a uniform distribution of spine number over the measured distance of the dendrite. These results are the first to indicate Tomo-1 protein has the capacity to regulate the genesis or stability of dendritic spines and, poten-

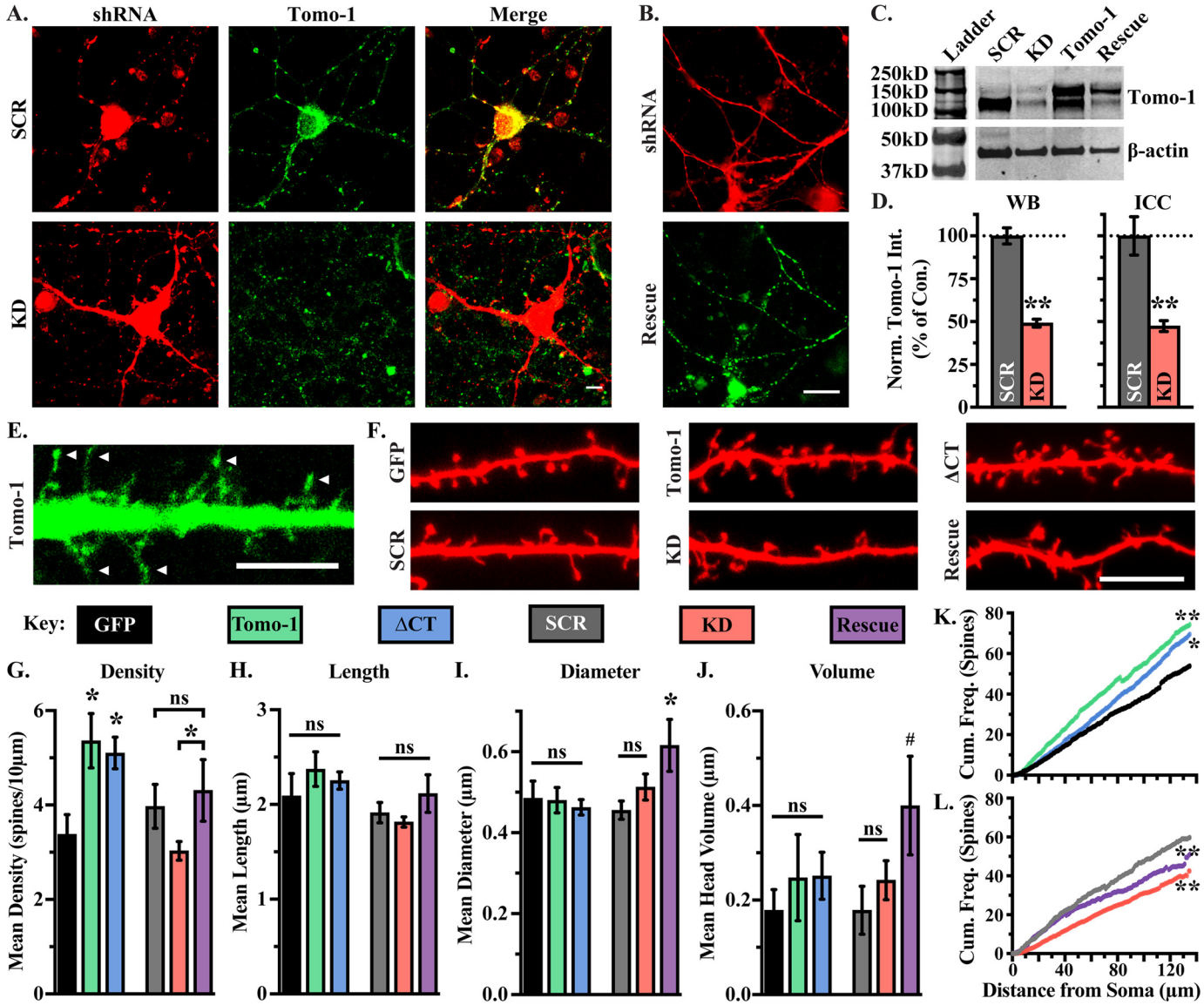

Figure 1. Effect of Tomo-1 protein abundance on dendritic spine density in hippocampal neurons. *A*, representative LSCM fluorescence micrographs of shRNA expression reporter (tRFP, *red*), Tomo-1 expression (anti–Tomo-1, *green*), and merged overlays in neurons following expression of the scrambled shRNA control (*SCR*) or an shRNA targeting Tomo-1 for KD. *Scale bar* = 10 μm. *B*, fluorescence micrographs of a neuron expressing Tomo-1 shRNA (*red*) + shRNA-resistant mCH-Tomo-1 (*green*, Rescue). *C*, comparison of Tomo-1 expression by Western blotting (20 μg/lane) following lentiviral infection with scrambled shRNA vector control (*SCR*), shRNA targeting Tomo-1 + GFP (*KD*), GFP Tomo-1 fusion protein (*Tomo-1*), or an shRNA-resistant mCherry-Tomo-1 (*Rescue*). *D*, lentiviral infection with an shRNA targeting Tomo-1 for knockdown (*red*) decreases Tomo-1 intensity to 49.1 ± 2.3% (by Western blotting, $n = 4$) and 47.4 ± 3.1% (via ICC, $n = 8$) of scrambled shRNA control vector (*gray*). *WB*, Western blotting. *E*, GFP Tomo-1 expression within a fixed dendrite indicates Tomo-1 overexpression localizes to dendritic spines (*white arrowheads*). *Scale bar* = 10 μm. *F*, representative fluorescence micrographs of dendrites in transfected neurons expressing cytosolic mCherry (*red*) and one of the following: GFP control (*GFP*, $n = 9$), GFP Tomo-1 (*Tomo-1*, $n = 8$), GFP Tomo-1 ΔCT, ($n = 13$), scrambled shRNA control (*SCR*, $n = 7$), Tomo-1 shRNA (*KD*, $n = 14$), or Tomo-1 shRNA + shRNA-resistant mCherry–Tomo-1 (*Rescue*, $n = 7$). *Scale bar* = 10 μm. *G–J*, averaged spine density (*G*), spine length (*H*), maximum spine head diameter (*I*), and spine head volume (*J*) for each indicated condition. *K* and *L*, comparison of cumulative frequency distributions of spine density in neurons in each condition. All data presented as population mean ± S.E., with *n* defined as individual dendrites or neurons from independent culture dishes. Statistical significance (#, $p < 0.1$; *, $p < 0.05$; **, $p < 0.01$), where indicated, was determined *versus* GFP or SCR vector controls using one-way ANOVAs with multiple comparisons of the mean or Kolmogorov-Smirnov tests of cumulative frequency distributions.

tially, the integrative synaptic drive of hippocampal neurons in culture.

Endogenous Tomo-1 co-localizes with PSD95 in dendritic spines

Next we examined by ICC if endogenous Tomo-1 is co-localized with the postsynaptic density protein PSD95, which may implicate its presence locally within spines of hippocampal neurons. Antigen specificity of the antibodies was confirmed by ICC of transfected HEK293T cells selectively overexpressing Tomo-1, Tomo-2, or empty vector control (Fig. 2*A*). Antibody specificity was further determined by Western blot analysis of transfected HEK293T cell lysates (Fig. 2*B*). As shown in Fig. 2*C*, ICC demonstrated that Tomo-1, although expressed throughout neurons, exhibits intense punctate immunofluorescence signals within neuronal processes. Although several prior reports have noted that Tomo-1 co-localizes with presynaptic markers, our results reveal Tomo-1 is also often found localized

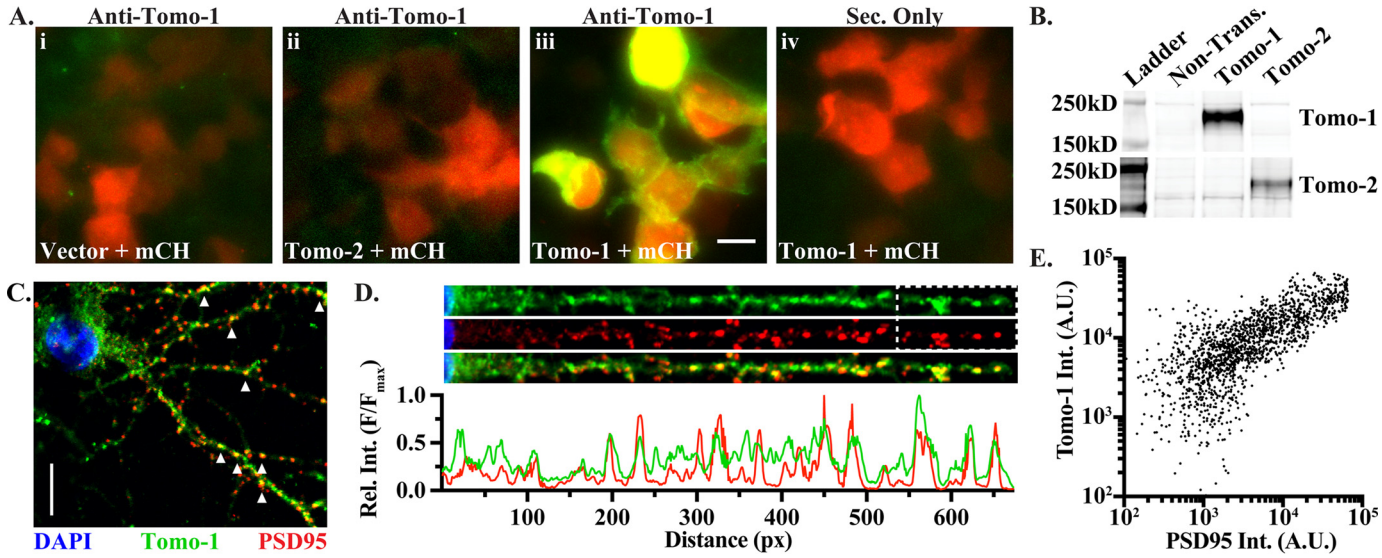

Figure 2. Tomo-1 localizes within postsynaptic compartments and is sensitive to shRNA-mediated knockdown. *A*, ICC of Tomo-1 (*green*) in HEK293T cells following expression of mCherry (*mCH*) (*red*) with (*i*) empty vector, (*ii*) Tomo-2, (*iii*) Tomo-1, or (*iv*) Tomo-1 (secondary antibody only). *Scale bar* = 10 μm. *B*, anti–Tomo-1 Western blot analysis of lysates from nontransfected HEK293T cells *versus* cells transfected with Tomo-1 or Tomo-2. *C*, representative ICC image of hippocampal neuron displaying merged fluorescence of endogenous Tomo-1 (*green*), PSD95 (*red*), and nuclei (*blue*, *DAPI*). *Scale bar* = 10 μm. *D*, representative intensity line scans of Tomo-1 (*green*) and PSD95 (*red*) fluorescence of an individual straightened dendrite indicate coincident immunofluorescence (*lower plot*). Merged Tomo-1 + PSD95 fluorescence (*lower micrograph*). *px*, pixels. *E*, cytofluorogram of Tomo-1 and PSD95 intensities from the *dashed box region* in *D* (Pearson's overlap coefficient, $r = 0.885$, $r^2 = 0.783$; Manders' correlation coefficients, M1 = 0.759, representing fraction of PSD95 overlapping Tomo-1, M2 = 0.889, representing fraction of Tomo-1 overlapping PSD95). *A.U.*, arbitrary units.

at postsynaptic sites, as indicated by co-localization of individual Tomo-1 and PSD95 immunofluorescent puncta (Fig. 2, *C*, *white arrowheads* and *D*, *top*). Indeed, line profiles of immunofluorescence along straightened dendrites show sites with highly correlated enrichment of Tomo-1 and PSD95 (Fig. 2*D*, *bottom*). Furthermore, pixel-by-pixel analysis of intensity profiles between the spectral channels further supports the validity of the observed co-localization between Tomo-1 and PSD95 (Fig. 2*E*, Pearson's overlap coefficient, $r = 0.885$, $r^2 = 0.783$; Manders' correlation coefficients, M1 = 0.759 (fraction of PSD95 overlapping Tomo-1), M2 = 0.889 (fraction of Tomo-1 overlapping PSD95)).

Proteasomal regulation of Tomo-1 determines its abundance

Because Tomo-1 expression level correlated with changes in dendritic spine density, we next evaluated if the UPS may dynamically regulate neuronal Tomo-1 levels. First, we tested the effects of inhibiting the proteolytic activity of the 26S proteasome complex via bath application of MG132 (50 μM, 4 h) or lactacystin (10 μM, 4 h) *versus* DMSO vehicle control. Proteasome blockade via either drug significantly increased neuronal Tomo-1 protein levels, as shown by Western blot analysis of whole-cell lysate samples (Fig. 3, *A* and *G*). Proteasome inhibition demonstrated no significant effect on total β-actin level. Depletion immunoprecipitation (IP) of Tomo-1 from lysate samples following proteasome blockade largely reproduced effects found on Western blotting input samples (Fig. 3, *B* and *H*). Specificity of the anti–Tomo-1 antibody used for IP was verified, as no immunoreactivity was apparent in Western blot analysis of rabbit IgG control or Tomo-2 immunoprecipitates (Fig. 3, *C* and *D*).

Tomo-1 interacts with the E3 ubiquitin ligase HRD1 in a proteasome activity–dependent fashion

HRD1 is an E3 ubiquitin ligase integral in the endoplasmic reticulum (ER) membrane (52). It is known to inhibit apoptosis following buildup of misfolded proteins and ER stress (53), and it is critical for ER-associated degradation (ERAD) (54). HRD1 protein is expressed in neurons, but not glia, of the hippocampus, dentate gyrus, and cerebral cortex (55), all of which also exhibit Tomo-1 protein expression (42, 56). Notably, HRD1 has previously been identified as an interacting partner of Tomo-2 in a proteomics screen of Tomo-2 IP from the INS1 pancreatic β-cell line, and was further reported to regulate Tomo-2 level when co-expressed in HEK293FT cells (43). Therefore, we next investigated if Tomo-1 interacts with HRD1 in hippocampal neurons, and if this is an E3-mediated mechanism by which Tomo-1 is specifically ubiquitinated and targeted for degradation. To test this, Tomo-1 was immunoprecipitated from neuronal lysates and the IP sample was tested for HRD1 co-precipitation. As shown in Fig. 3*B*, Tomo-1 IP resulted in co-precipitation of HRD1. As control, IP with anti-rabbit IgG, resulted in no Tomo-1 or HRD1 immunoreactivity (Fig. 3*C*). To date, most known Tomo-1 protein interactions have been reported to occur via its R-SNARE domain, which is homologous to the R-SNARE of VAMP2. However, as shown in Fig. 3*E*, IP of VAMP2 from neuronal cultures failed to co-immunoprecipitate HRD1, indicating that the Tomo-1 SNARE motif is unlikely a domain essential for interaction between Tomo-1 and HRD1. Although the UPS inhibitors MG132 and lactacystin increased Tomo-1 level in neuronal cultures, no significant increase in the level of HRD1 occurred following these treatments (Fig. 3, *F* and *I*). Importantly, however, proteasome blockade increased the extent to which HRD1 co-precipi-

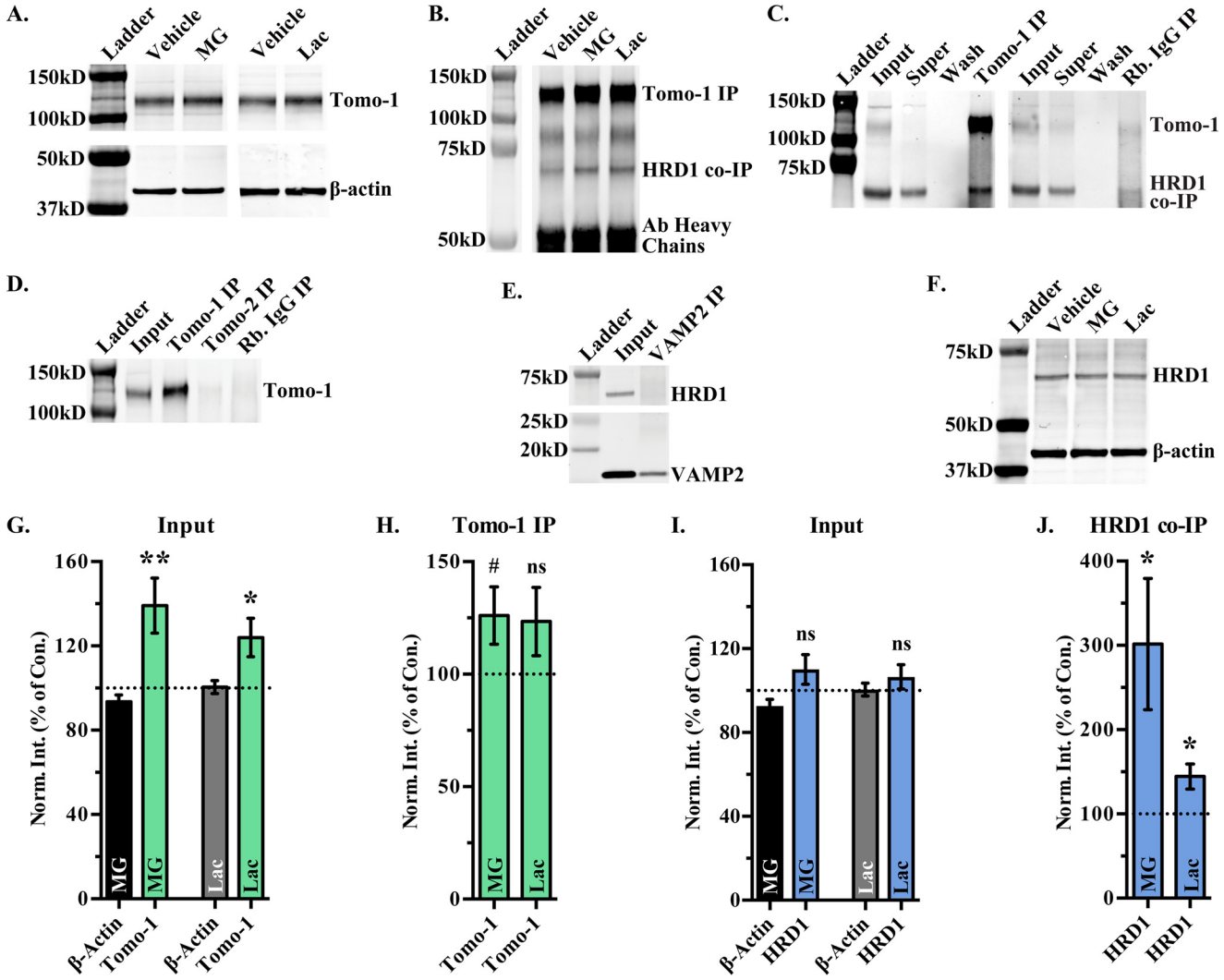

Figure 3. Effect of proteasome blockade on neuronal Tomo-1 protein and its interaction with the E3 ligase HRD1. *A*, Western blotting analysis of neuronal cultures treated with proteasome inhibitors MG132 (*MG*) (50 μM, 4 h) or lactacystin (*Lac*) (10 μM, 4 h) *versus* DMSO vehicle control on endogenous Tomo-1 protein levels. *B*, Western blotting analysis of proteasome treatments, as in part *A*, on Tomo-1 IP and HRD1 co-IP levels. *C*, IP of Tomo-1 co-IPs HRD1, however IgG control IP does not co-immunoprecipitate HRD1. Tomo-1 was immunodepleted from lysates (*Input*), with little immunoreactive Tomo-1 in post-IP supernatant (*Super*). *D*, the Tomo-1 antibody is selective for precipitating Tomo-1 protein from lysates as Tomo-1 IP (15 DIV, 20 μg/sample), but not rabbit IgG control (*Rb. IgG*) or Tomo-2, showed Tomo-1 immunoreactivity. *E*, IP of VAMP2 does not result in co-IP of HRD1. *F*, treatment of cultures with the proteasome inhibitors, as in *A*, resulted in no significant change in endogenous HRD1 in lysate. Data are normalized against β-actin protein levels (*MG*, $n = 7$; *Lac*, $n = 7$). *G*, quantification of Tomo-1 inputs from *A* (normalized to β-actin protein levels; *MG*, $n = 28$; *Lac*, $n = 21$). *H*, quantification of Tomo-1 IPs from *B*. Averages are presented as percent change *versus* vehicle-treated controls (*dotted line*; *MG*, $n = 7$; *Lac*, $n = 7$). *I* and *J*, quantification of HRD1 from lysate inputs (*I*) and HRD1 co-IP with Tomo-1 (*J*) (*MG*, $n = 6$; *Lac*, $n = 7$). All data presented as population mean ± S.E., with *n* defined as independent neuronal culture dishes. Statistical significance (#, $p < 0.1$; *, $p < 0.05$; **, $p < 0.01$), where indicated, was determined using two-tailed *t*-tests.

tated with endogenous Tomo-1 (Fig. 3, *B* and *J*). These results indicate that perturbation of proteasome activity–dependent regulation not only affects Tomo-1 protein level, but may also alter the extent to which Tomo-1 interacts with HRD1.

HRD1 is present in neuronal processes and synapses

Because mammalian HRD1 is localized to the ER membrane, we next examined by ICC if HRD1 is present within neuronal processes, such as dendrites, where it may possess the ability to ubiquitinate and spatially regulate postsynaptic Tomo-1. Indeed, the ER has been reported to extend from somatic areas, where it is heavily enriched, into dendritic shafts and spines of neurons (57). Furthermore, localized ER stress responses have been detected in dendrites of cultured mouse hippocampal neurons (58). As shown in Fig. 4*A*, ICC of HRD1 in neuronal cultures demonstrated extensive HRD1 immunofluorescence within somata, as expected, but notably also within neuronal processes (Fig. 4, *A* and *B*). A fluorescence intensity alignment profile of HRD1 and PSD95 along straightened dendrites demonstrated localization within processes (Fig. 4*B*, *bottom*). However, the diffuse dendritic distribution of HRD1 suggested it was not specifically located at sites of PSD95 fluorescent puncta (Fig. 4*C*, Pearson's overlap coefficient, $r = 0.437$, $r^2 = 0.191$; Manders' correlation coefficients, M1 = 0.724 (fraction of PSD95 overlapping HRD1), M2 = 0.517 (fraction of HRD1 overlapping PSD95)).

The finding of an ER-localized E3 ligase within dendrites of primary hippocampal neurons suggests that HRD1 regulation of Tomo-1 may occur beyond the somatic compartment. As

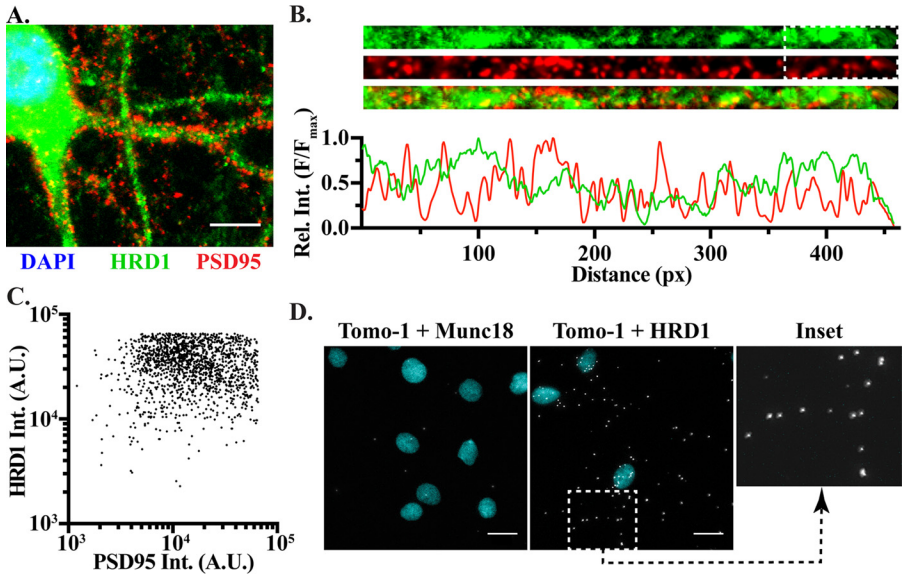

Figure 4. The E3 ligase HRD1 is present throughout neuronal processes and interacts with Tomo-1. *A*, representative ICC image showing merged immunoreactive fluorescence of endogenous HRD1 (*green*), PSD95 (*red*), and nuclei (DAPI, *blue*) in cultured neurons. *Scale bar* = 10 μm. Note presence of HRD1 in dendrites. *B*, representative fluorescence intensity line scans of HRD1 (*green*) and PSD95 (*red*) of an individual straightened dendrite indicate coincident immunofluorescence (*lower plot*). Merged Tomo-1+PSD95 fluorescence is also shown (*lower micrograph*). *px*, pixels. *C*, cytofluorogram analysis of fluorescence intensity relationship between HRD1 and PSD95 from *dashed box* region on dendrite highlighted in *B* (Pearson's overlap coefficient, $r = 0.437$, $r^2 = 0.191$; Manders' correlation coefficients, M1 = 0.724, representing fraction of PSD95 overlapping HRD1; M2 = 0.517, fraction of HRD1 overlapping PSD95), indicates a lack of specific co-localization. *A.U.*, arbitrary units. *D*, representative Tomo-1 and HRD1 interaction assessed via proximity ligation analysis demonstrates substantive numbers of fluorescent puncta in somatic regions and along neuronal processes (12 DIV). *Scale bar* = 10 μm. *Inset* expands outlined region. PLA testing for interaction between Tomo-1 and the synaptic protein Munc18 (*top*) resulted in low levels of fluorescent puncta similar to secondary antibody treatment alone (not shown).

such, we next investigated if interaction between endogenous Tomo-1 and HRD1 proteins occur in neurons, including processes, using a proximity ligation assay (PLA) in fixed cultures. Interestingly, PLA fluorescent puncta indicated that Tomo-1 and HRD1 interact within the somata and nonsomatic regions (Fig. 4, *D* and *inset*). Specificity of this PLA interaction was demonstrated by the absence of a PLA signal when an interaction between Tomo-1 and the cytosolic exocytic regulatory protein Munc18 was tested. Furthermore, fluorescent puncta were not apparent in antibody omission control PLA reactions (data not shown).

Tomo-1 protein is ubiquitinated prior to proteasomal degradation

To determine whether Tomo-1 is subject to HRD1-mediated ubiquitination within neurons, we next infected neuronal cultures with an N-terminal–tagged YFP Tomo-1 fusion protein, which efficiently precipitated with an anti-GFP nanobody (Fig. 5*A*). Importantly, IP samples from the YFP Tomo-1–expressing neurons demonstrated ubiquitinated YFP Tomo-1 conjugates (Fig. 5*B*). Conjugated ubiquitin immunoreactivity was not apparent in IP samples of the Tomo-1 knockdown condition, in which cytosolic GFP was co-expressed. Furthermore, with GFP expression (Fig. 5*C*, *top*) no ubiquitin immunoreactivity was observed at 26 kDa, the molecular mass of GFP-family proteins, following GFP IP (Fig. 5*C*, *bottom*). This finding indicated that Tomo-1, and not the YFP (a GFP point mutant) fluoroprotein, was ubiquitinated.

We next examined if ubiquitination of the exogenously expressed YFP Tomo-1 was altered by pharmacological proteasome blockade. As shown in Fig. 5, *D–F*, the expression level of YFP Tomo-1 was increased by ~1.5-fold *versus* DMSO vehicle control after a 4-h treatment with either MG132 or lactacystin. To mitigate deubiquitination in these experiments the broad-spectrum deubiquitinating enzyme inhibitor PR-619 was co-applied with proteasome inhibitors. Fig. 5, *E* and *G* show that the increase in Tomo-1 level following proteasome blockade was accompanied by a significant increase in Tomo-1 ubiquitination, and, notably, the co-immunoprecipitation (co-IP) of HRD1 with YFP Tomo-1 also increased upon MG132 treatment. Importantly, the fraction of Tomo-1 that was ubiquitinated following proteasome blockade significantly increased relative to total Tomo-1 IP level.

HRD1 ubiquitinates Tomo-1 to regulate its level

To determine whether HRD1 is capable of directly ubiquitinating Tomo-1 we utilized an *in vitro* ubiquitination assay. For this assay, we expressed and affinity-purified Tomo-1 protein from HEK293T cells, and used commercially available purified HRD1 and its various upstream cofactors (ubiquitin, UBE1, UBE2D2, and ATP). As shown in Fig. 5*H*, Tomo-1 is ubiquitinated in a concentration-dependent fashion by HRD1. Moreover, significant ubiquitination above background did not occur in control conditions lacking HRD1, Tomo-1, or ATP, or when testing the empty vector control expressed and purified in the same manner as Tomo-1. Replacement of either the upstream E2 ubiquitin-conjugating enzyme (with UBE2G2), or the HRD1 itself (by another E3 enzyme of the same RING-type class: CHIP/STUB1) failed to induce Tomo-1 ubiquitination (data not shown).

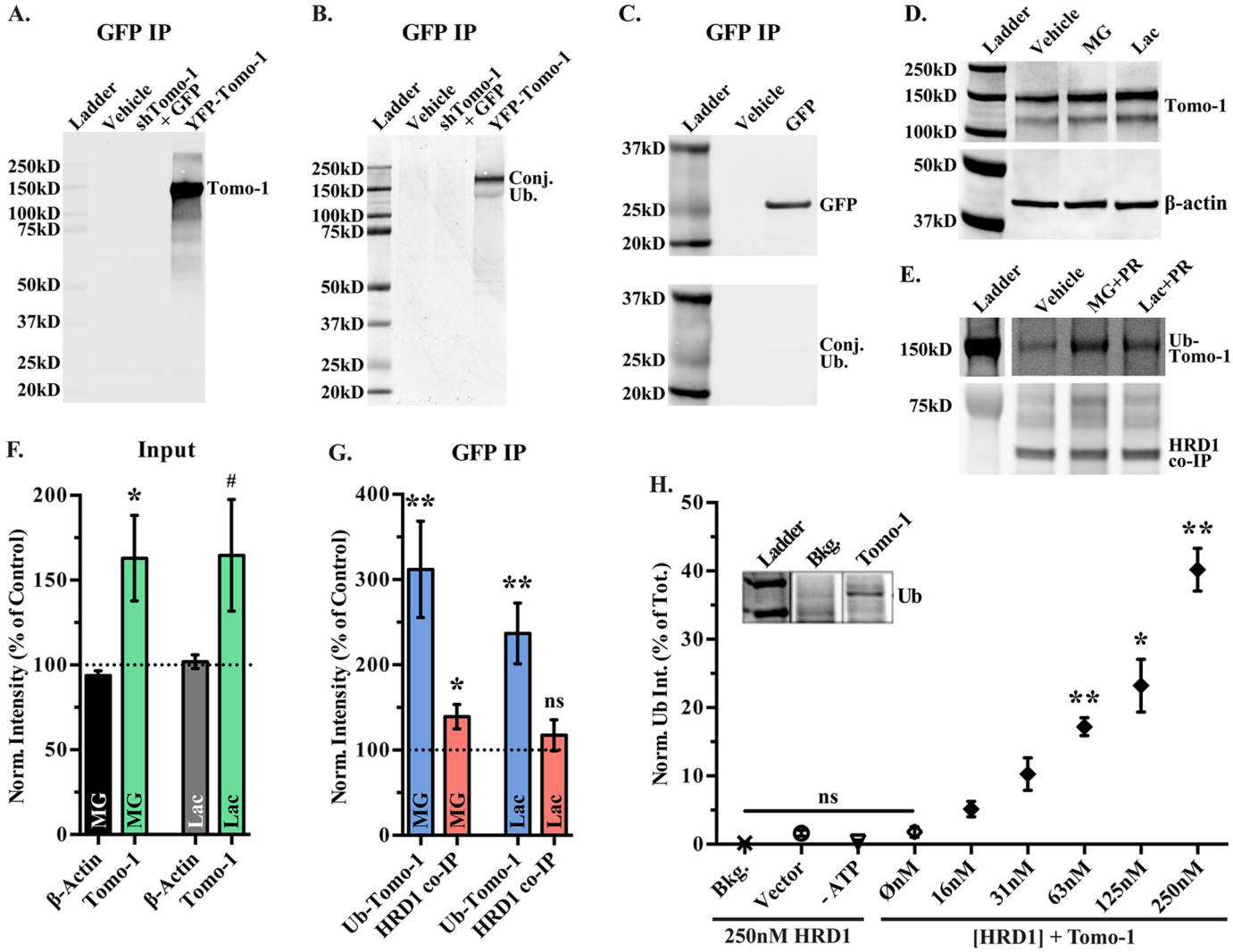

Figure 5. Tomo-1 in hippocampal neurons is subject to *in situ* ubiquitination and is ubiquitinated *in vitro* by HRD1. *A* and *B*, Western blotting of YFP Tomo-1 IP from lentivirus-infected neurons were probed for immunoreactivity against Tomo-1 (*A*) and conjugated-ubiquitin (*Conj. Ub.*) (*B*). *B*, neuronal infection with a lentivirus expressing shTomo-1 and free GFP demonstrated no anti–conjugated ubiquitin reactivity at 26 kDa. *C*, Western blotting of GFP (*top*) and conjugated ubiquitin (*bottom*) following GFP IP from infected neurons. *D*, Western blotting for endogenous Tomo-1 and expressed YFP Tomo-1 from lysates of neurons following treatment with the proteasome inhibitors MG132 (*MG*, 50 μM, 4 h) or lactacystin (*Lac*, 10 μM, 4 h). *E*, Western blotting of Tomo-1 IP probed for conjugated ubiquitin (*top*) and for HRD1 (*bottom*) following treatment with proteasome inhibitors plus 10 μM PR-619 (*PR*). *F*, averaged YFP Tomo-1 and β-actin levels from *D* (*MG*, $n = 18$; *Lac*, $n = 13$). *G*, averaged ubiquitinated Tomo-1 level and HRD1 co-IP levels from *E* (*MG*, $n = 10$; *Lac*, $n = 8$). Above data (*F* and *G*) presented as population mean ± S.E., with *n* defined as independent neuronal culture dishes. Averages are expressed as percent change relative to paired, vehicle-treated experimental controls (*dotted line*). Statistical significance (#, $p < 0.1$, *, $p < 0.05$, **, $p < 0.01$) was determined using two-tailed *t*-tests. *H*, concentration-dependent *in vitro* ubiquitination of purified Tomo-1 by HRD1. *Inset* displays anti-ubiquitin Western blotting of representative reaction product. Data are expressed relative to background and negative controls with significance (*, $p < 0.05$; **, $p < 0.01$; $n = 3$) determined via multiple comparisons ANOVA. *Bkg.*, background.

HRD1 degrades Tomo-1 to increase dendritic spine density

We next investigated if HRD1 ubiquitination and proteasomal targeting of Tomo-1 may modify the density of dendritic spines. To address this question we tested shRNA constructs for HRD1 KD, and examined their effect on endogenous Tomo-1 protein level in hippocampal neuronal cultures. Two lentivirus-driven shRNAs targeting nonoverlapping regions of HRD1 mRNA were tested. The shHRD1 constructs resulted in significant (39 and 47%) decreases in HRD1 protein level relative to a scrambled shRNA control, as determined by Western blot analysis of whole cell lysate samples (Fig. 6*A*). The incomplete KD of HRD1 within these neuronal lysates was likely the result of an only 56% transduction efficiency in cultured neurons (Fig. 6*B*). This suggests that the level of HRD1 within infected neurons may be lower than 50% of control. Viral infection was highly specific to neurons, as evidenced by neuronal-specific nuclei labeling with anti-NeuN. Our incomplete knockdown of HRD1 is of similar extent to previously reported RNAi-based knockdown of HRD1 in differentiated neurons (59). However, utilizing ICC fluorescence imaging to assess HRD1 KD efficiency, we observed that HRD1 fluorescence intensity levels in cells infected with a 50:50 mixture of both HRD1 shRNAs decrease ~72.2% as compared with SCR controls (Fig. 6, *C* and *D*). Notably, the decrease found via Western blot analysis of HRD1 protein level following 52.5% knockdown resulted in a significant increase in Tomo-1 protein level by an average of 140.6% of control (Fig. 6, *E* and *F*).

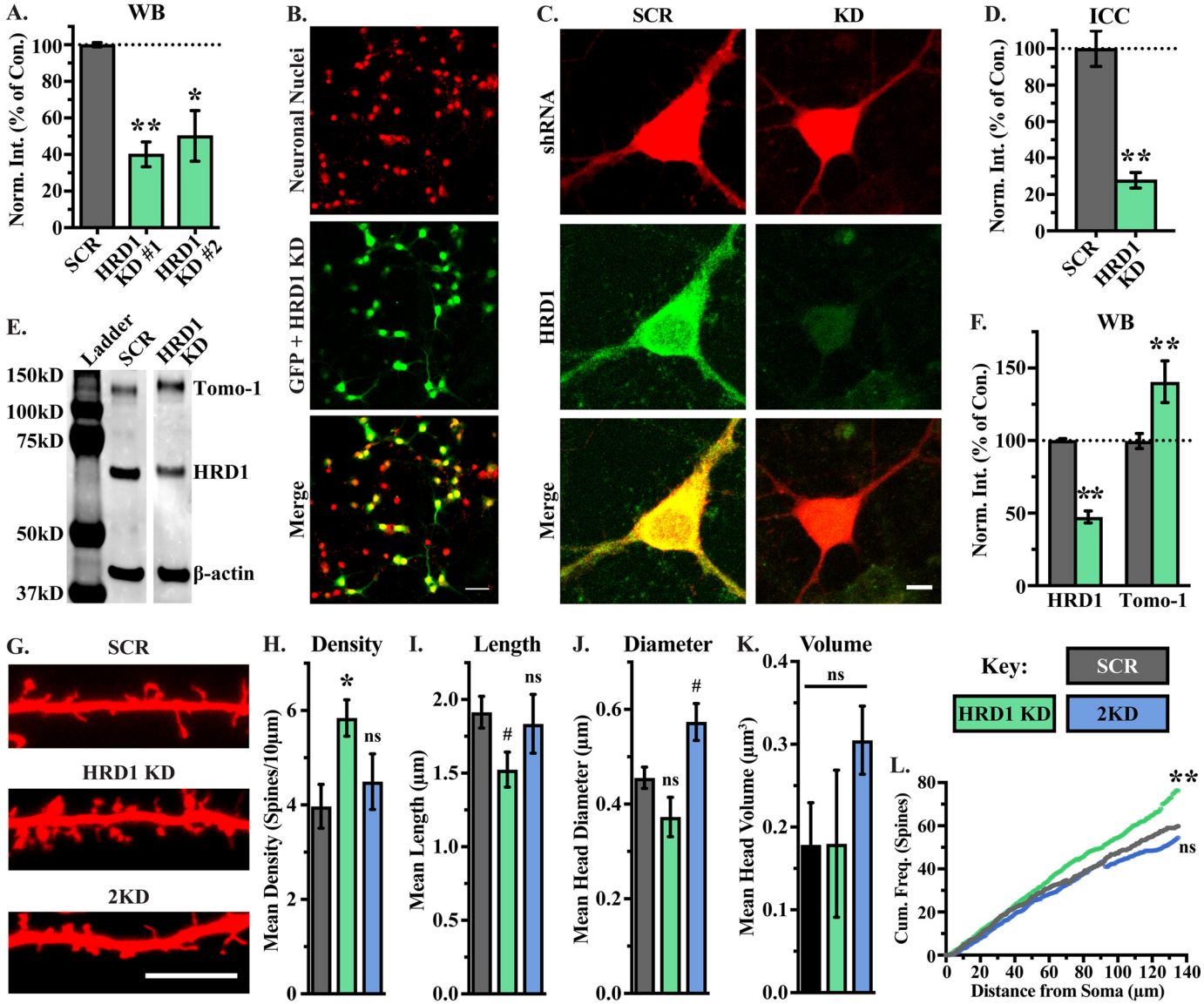

Figure 6. Effect of HRD1 on dendritic spine density and functional relationship to Tomo-1. *A*, histograms of shRNA-mediated decreases in HRD1 from virally transduced cultures with two different shRNA KD sequences targeting HRD1 (mean ± S.E., multiple comparisons ANOVA, *, $p < 0.05$; **, $p < 0.01$; $n = 3$). *WB*, Western blotting. *B*, representative images of shHRD1-infected neuronal cultures. Transduction efficiency was quantified by counting shHRD1-expressing neurons (GFP + HRD1 KD, *middle*) *versus* the total number of neurons present (anti-NeuN, *top*). Transduction efficiency averaged 56%, with <8% non-neuronal infection ($n = 1972$ neurons, 20 fields of view, four dishes). *Scale bar* = 50 μm. *C*, representative LSCM fluorescence micrographs of shRNA expression reporter (tRFP, *red*), HRD1 expression (anti-HRD1, *green*), and merged overlays in neurons following expression of the scrambled shRNA control (*SCR*) or an shRNA targeting HRD1 for KD, as in *B*. *Scale bar* = 10 μm. *D*, histograms of shRNA-mediated decrease in HRD1 level following ICC of cultures infected with a 1:1 ratio of both HRD1 shRNA KD vectors. Values (mean ± S.E., $n = 9$) are normalized to anti-HRD1 ICC signal in scrambled shRNA (*SCR*) infected neurons. *E*, Western blotting comparison of neuronal HRD1 expression between lentiviral-infected SCR and HRD1 shRNA KD. *F*, histogram comparing HRD1 and Tomo-1 expression levels in neuronal cultures treated with a mix of the HRD1 KD shRNAs (*green*) or SCR control (*gray*). Statistical significance (**, $p < 0.01$; mean ± S.E.; HRD1, $n = 17$; Tomo-1, $n = 14$) was determined using multiple *t*-tests. *WB*, Western blotting. *G*, representative LSCM fluorescence micrographs of dendrites emanating from cultured hippocampal neurons transfected with and expressing cytosolic mCherry (*red*) and HRD1 shRNA (*HRD1 KD*), or Tomo-1 shRNA + HRD1 shRNA (*2KD*). *Scale bar* = 10 μm. *H–K*, comparison of averaged spine density (*H*), spine length (*I*), spine head maximum diameter (*J*), and spine head volume (*K*) of individual neurons (14–28 DIV) for the following conditions: HRD1 KD (*green*, $n = 7$), SCR control (*SCR*, *gray*, $n = 7$), or shRNAs targeting both HRD1 and Tomo-1 (*2KD*, *blue*, $n = 8$). *L*, cumulative frequency distributions of spine density from above conditions.

We next investigated the effects of HRD1 KD on dendritic spines, to determine whether the effects of Tomo-1 on spine density are dependent upon regulation by HRD1. We performed confocal imaging and 3D reconstruction and analysis of dendritic spines as in Fig. 1. First, neuronal cultures were transfected with a soluble mCherry fluorophore and co-transfected with either; shRNAs targeting HRD1 (HRD1 KD), or the scrambled shRNA vector. Each shRNA construct co-expresses a soluble GFP reporter fluorophore. Representative images for each condition are shown in Fig. 6*G*. HRD1 KD was found to significantly increase average spine density, from 3.9 to 5.8 spines per 10 μm, relative to the SCR control (Fig. 6*H*). This effect parallels that observed following Tomo-1 overexpression, suggesting that HRD1 may tune spine density via Tomo-1 ubiquitination and targeting for degradation. Effects of HRD1 KD exhibited a statistically significant on average spine length, but no effect was found on head diameter or volume (Fig. 6, *I–K*). Cumulative spine frequency in the HRD1 KD was similar to the change

observed for Tomo-1 overexpression (significant increase *versus* respective controls) (Fig. 6*L*). We next tested if the alteration in spine density or cumulative spine frequency following HRD1 KD is related to specific actions of HRD1 on Tomo-1. This was assessed by simultaneous shRNA-mediated knockdown of Tomo-1 and HRD1. Importantly, the effect of HRD1 KD to increase average spine density was nearly completely blocked in the double KD condition (2KD) (Fig. 6*H*). The 2KD condition also exhibited a significant increase in averaged spine head diameter, with an accompanying trend on spine head volume but not spine length (Fig. 6, *I–K*). These data suggest that the actions of HRD1 on spine density occur directly on or within the Tomo-1 signaling pathway, which itself alters spine density.

Discussion

In the present study, we identify Tomo-1, a soluble R-SNARE motif–containing protein, as a novel positive regulator of the density of dendritic spines in cultured hippocampal neurons. Tomo-1 overexpression specifically increased dendritic spine density without influencing average spine length, maximum head diameter, or head volume. Conversely, Tomo-1 knockdown decreased dendritic spine density. Notably, we have also determined that Tomo-1 is an interacting partner of and a specific target substrate for ubiquitination by the E3 ligase HRD1, which subsequently promotes Tomo-1 degradation by the 26S proteasome. Ablation of HRD1 activity via targeted knockdown increased global Tomo-1 protein levels in cultured neurons. Furthermore, HRD1 knockdown increased dendritic spine density. This effect was blocked following simultaneous knockdown of HRD1 and Tomo-1, strongly suggesting a signaling pathway involving both proteins in determining spine density. Thus, our data show that HRD1-mediated regulation of Tomo-1 is a newly identified component in neuronal regulation of spine density by the UPS and, therefore, potentially on synaptic dynamics of hippocampal neurons.

Neurons are highly polarized cells, with complex regulatory mechanisms that control cell excitability, synaptic plasticity, and information transfer within the brain. Tomo-1 has conserved orthologs (60) across a diversity of organisms and systems, demonstrating their important function in membrane trafficking and intercellular signaling. In addition, Tomo-1 exhibits a low level of genic intolerance relative to that expected by neutral variation found in genes (RVIS −0.4 (27%)) (61), suggesting that genetic variants of Tomo-1 may confer an increased risk of disease. Functionally, Tomo-1 has inhibitory actions on secretion within the brain (17), superior cervical ganglion neurons (36), bovine adrenal chromaffin cells (62), pancreatic β-cells (25), and in PC12 (40, 63) and CHO (64) cell lines. The most commonly reported mechanism of Tomo-1 action has been its role in inhibiting the priming and concomitant fusion of the readily releasable pool (RRP) of vesicles in neurons (19, 30, 65) and neuroendocrine cells (66). In addition to Tomo-1 actions on the RRP, Tomo-1 has recently been shown to control the proportional reallocation of neurotransmitter-containing vesicles between functionally identified presynaptic vesicle pools (30).

The current study identifies a completely novel postsynaptic effect of Tomo-1, the regulation of dendritic spine density in cultured hippocampal neurons. Interestingly, this action of Tomo-1 occurs independently of its C-terminal R-SNARE domain. The effects of Tomo-1 on dendritic spines may be analogous to known membrane trafficking and cytoskeletal regulation roles mediated by Tomo-1 orthologs. For example, two yeast Tomo-1 proteins, Sro7p/77p, together with Sec4 and Myo2 (18, 67–69), modulate exocytosis by associating with cytoskeletal components and regulating SNARE function on the plasma membrane (31, 37).

The key importance of Tomo-1 in orchestrating vesicle priming and exocytotic secretion of chemical messengers raises an imperative need to identify and characterize the signaling pathways which control it. However, identification of transcriptional, translational, and degradative mechanisms mediating the expression level of Tomo-1 and, therefore, the dynamic range of its activity in neurons, is lacking. The present study has uncovered a novel form of Tomo-1 protein regulation in central neurons via the ubiquitin-proteasome system. We have identified HRD1, an ER-resident RING-type E3 ubiquitin ligase, as a novel upstream regulator which specifically targets Tomo-1 for degradation. Indeed, PLA imaging data indicated that although endogenous Tomo-1 and HRD1 are abundant in the cell soma they also generally appear to be overlapping within neuronal dendrites. Further, HRD1 was co-immunoprecipitated with Tomo-1 from neuronal lysate, and *in vitro* reactions using purified HRD1 and Tomo-1 proteins demonstrated concentration-dependent Tomo-1 ubiquitination by HRD1. The potential for similar actions occurring *in vivo* is supported by our results demonstrating that pharmacological proteasome blockade, via bath application of MG132 or lactacystin, increased neuronal Tomo-1 protein level. Moreover this action occurred on a shorter time scale than the half-life of most synaptic proteins (70), suggesting that ubiquitination may be used to selectively target Tomo-1 for rapid proteasomal degradation. However, future consideration is warranted for the concurrent examination of Tomo-1 biosynthetic activity, as production rates may be linked to reduced UPS-mediated degradation or actions of proteasome blockers.

A proteomics screen of pulldown samples of Tomo-2 from the insulin-secreting INS1 β-cell line also identified HRD1 as one of the highest confidence Tomo-2 interacting partners, in addition to HRD1 adaptor proteins (43). It is currently not known at which lysine residues Tomo-1 is ubiquitinated by HRD1, nor to what extent ubiquitination alters the half-life of Tomo-1. Nonetheless, HRD1's well-established function in ubiquitinating target substrates for proteasomal degradation during ER-associated degradation can now be expanded to include actions within dendrites and on synaptic proteins. In addition, as Tomo-1 and HRD1 co-localize to dendrites where they likely interact, the potential exists for localized regulation of Tomo-1 protein level within, or near, postsynaptic sites. A rapid, potentially local, degradation of Tomo-1 may occur in a similar fashion to dephosphorylation-induced, UPS-mediated degradation of fragile X mental retardation protein (FMRP) in the dendrites and synapses of cultured rat neurons (71).

Specific E3 ubiquitin ligases are known to influence synaptic physiology and plasticity in both nonproteolytic (72) and proteolytic-dependent manners (73). Some of these have been shown to be dependent upon postsynaptic activity (11, 74, 75). Spine morphogenesis and number (76), as well as spine maintenance (77), including specific AMPA receptor subunit levels and membrane integration (78), are tightly controlled by the UPS. Within the microenvironment of the synapse, targeted protein degradation involving many specific E3 ubiquitin ligases, confers substrate specificity in ubiquitination. Indeed, numerous neuronal E3s have been identified that functionally regulate specific levels of postsynaptic proteins. These include γ-actin (79), GKAP, and Shank (80), which are regulated by TRIM3, PSD95 by Mdm2 (13) upon facilitation by CDK5 (81), AMPARs by RNF167 (82), and the postsynaptic cytoskeletal protein and immediate early gene Arc by both UBE3A (83) and RNF216/TRIAD3 (84). Targeted ubiquitination of presynaptic proteins is also prominent. For example, the active zone (AZ) protein RIM1, which scaffolds the multiprotein modules which regulate priming and release of neurotransmitter-containing vesicles, is acted upon by the E3 ligase SCRAPPER and results in rapid alteration in presynaptic release (85). Furthermore, the active zone proteins Bassoon and Piccolo, which are subject to regulation by the E3 ligase Siah1, were shown to be crucial in the ubiquitination and maintenance of numerous presynaptic proteins (8).

Prior reports have identified HRD1 as important in regulating neuronal cell biology. For example, up-regulation of HRD1 following ER stress in differentiated neurons decreases neurite outgrowth and dendritic arborization (59). Furthermore, HRD1 has been shown to promote the degradation of other components of the synaptic proteome, including the Parkin-associated endothelin receptor–like receptor, PaelR (55), and expanded polyglutamine variants of Huntingtin (86). Our results indicate that HRD1, which is well-known to act on membrane delimited proteins, also regulates the cytosolic protein Tomo-1. Although HRD1 targeting of soluble proteins has been rarely reported, it has been shown to facilitate proteasomal degradation and aggresome formation of Optineurin (87), a cytosolic protein involved in the maintenance of the Golgi complex, membrane trafficking, and exocytosis. Interestingly, Optineurin, like the Tomo-1 orthologs Sro7p/77p, is reported to interact with myosin and Rab family proteins (31, 38, 88).

E3 ligase–mediated ubiquitination of substrate proteins is often sensitive to the state of the target protein's post-translational modifications (PTMs). Tomo-1 is regulated via multiple modifications, including phosphorylation at specific amino acid sites by PKA (36), Akt/PKB (64), and CDK5 (30) kinases, in addition to SUMOylation (40), which is mediated by the E3 PIAS (41). Furthermore, there is a growing body of evidence indicating facilitated co-regulation of protein substrates by phosphorylation, ubiquitination, and other PTMs. For example, CDK5, a kinase recently reported to phosphorylate Tomo-1 and exert a functional impact on the RRP, is down-regulated following the *S*-nitrosylation of its upstream activator p35. This causes p35 ubiquitination by the E3 PJA2 and degradation (89). Although the physiological signal driving HRD1-mediated ubiquitination of Tomo-1 is unknown, it may result from up- or down-regulated PTM of Tomo-1, or indirectly following the PTM of kinases and other upstream Tomo-1 regulators. Such integrative mechanisms may serve to balance the rate and targets of degradation and also provide the possibility for diversity in subcellular localization and activity dependence.

Ubiquitination and proteasomal degradation of synaptic proteins does not necessarily indicate an impact on plasticity. It is currently unknown if the relationship between Tomo-1 and HRD1 is regulated following neuronal activity, for example, in a homeostatic fashion. TOM-1, a Tomo-1 ortholog in *C. elegans* was, however, reported to increase presynaptically in response to neurexin/neuroligin-mediated retrograde down-regulation of presynaptic neurotransmitter release (39). The molecular mechanism driving the change in TOM-1 protein level remains uncharacterized. Furthermore, we have previously shown that Tomo-1 contributes to CNQX-induced synaptic scaling in hippocampal neurons (30), a form of homeostatic plasticity occurring following synaptic inactivation via AMPAR blockade. Future investigations are required to address the physiological parameters regulating HRD1-mediated Tomo-1 ubiquitination and the resulting functional consequences.

Experimental procedures

Animals

All animal handling procedures are approved by and in full compliance with the regulations of the Institutional Animal Care & Use Committee (IACUC) of the University of Michigan, in addition to the National Institutes of Health guidelines.

Antibodies

Affinity-purified Rb anti-Tomosyn-1 polyclonal antibody (catalogue no. 183103), affinity-purified Rb anti-Tomosyn-2 polyclonal antibody (catalogue no. 183203), and the Ms anti-PSD95 monoclonal antibody (catalogue no. 124011) were from Synaptic Systems (Gottingen, Germany). The Ms anti–β-actin monoclonal antibody (clone AC74, catalogue no. A2228) was from Sigma-Aldrich. The Rb anti-HRD1 polyclonal antibody (catalogue no. 13473-1-AP) was from Proteintech (Chicago, IL). The Ms anti-conjugated-ubiquitin monoclonal antibody (clone FK2, catalogue no. BML-PW8810) was from Enzo Life Sciences (Farmingdale, NY). The Ms anti-GFP antibody (clone C163, catalogue no. 33-2600) was from Thermo Fisher. For Western blotting, IRDye 800CW-conjugated goat anti-mouse IgG H+L (catalogue no. 926-68021) and IRDye 680LT-conjugated goat anti-rabbit IgG H+L (catalogue no. 926-32210) fluorescent secondary antibodies were from LI-COR Biosciences (Lincoln, NE). For light microscopy immunocytochemistry Alexa Fluor 488-, 594-, and 647-conjugated species-specific anti-IgG secondary antibodies raised in goat (catalogue nos. A11073, A11012, and A21236, respectively) were from Invitrogen. Affinity-purified Ms anti-NeuN (neuronal nuclei) monoclonal antibody (clone A60, catalogue. no. MAB377) was from EMD Millipore (Billerica, MA).

Cell culture and transfections

All results were obtained from dissociated rat hippocampal neuronal cultures (17–28 DIV), unless otherwise noted. Hip-

pocampal neuronal cultures were prepared as previously described, with minor adjustments (90). Briefly, hippocampal neurons from embryonic day 19–20 Sprague-Dawley rats of either sex (Charles River) were plated at 400–450 cells/mm^2 on either 18-mm diameter, no. 1.5 thickness coverglass (Neuvitro, catalogue no. GG-18) or on 14-mm microwell glass-bottom 35-mm culture dishes (MatTek (Ashland, MA), catalogue no. P35G-0.170-14-C) and maintained in an incubator containing 95%/5% O_2/CO_2 and 100% humidity at 37 °C in NBActiv4 medium (catalogue no. Nb4, BrainBits, Springfield, IL) for up to 4 weeks *in vitro* prior to experimentation. Half of the neuronal culture medium was replaced every 3–4 days until experimentation.

Hippocampal cultures were co-transfected at 13–21 DIV for spine imaging at 17–25 DIV. Transfection was achieved using 200 μl of NBActiv4, including 1 μl Lipofectamine 2000 (Invitrogen, catalogue no. 11668019) per dish and pCAG-mCherry (0.4 μg/dish), in addition to one of the following constructs (1 μg/dish): GFP shTomo-1, GFP shHRD1, GFP shSCR, GFP Tomo-1, GFP Tomo-1 lacking the C terminus. Transfection solutions were allowed to stand for 30 min before being dripped onto the cell cultures. Cultures were incubated for 1 h with the Lipofectamine/DNA mix, after which media were exchanged with fresh NBActiv4 media. Pyramidal neurons were then imaged 3–5 days post-transfection.

HEK293T cells (catalogue no. CRL-3216, ATCC, Manassas, VA, ≤15 passages) were seeded in plastic T-75 tissue culture flasks at <75% confluence in an incubator containing 95%/5% O_2/CO_2 and 100% humidity at 37 °C in DMEM (Gibco catalogue no. 11960) containing: 10% FBS (Gibco catalogue no. 10437-028), 1% GlutaMAX (Thermo Fisher, catalogue no. 35050061), 1% penicillin-streptomycin (Sigma, catalogue no. P4333), and 1% nonessential amino acids (Gibco, catalogue no. 11140–050).

Cloning of full-length rat m–Tomo-1 constructs into the Gateway Expression vector

The coding sequence of rat m-Tomosyn-1 (NCBI accession number NP_110470.1) was cloned into the NativePure Gateway destination vector pcDNA3.2/capTEV-CT/V5-DEST (Invitrogen, catalogue no. BN3002) for expression in HEK293T cells and native affinity purification for use in the *in vitro* ubiquitination reactions.

Drugs

The following chemicals were used for this study, as noted: DMSO (Life Technologies, catalogue no. D12345), MG132 (Cayman Chemicals, catalogue no. 10012628), lactacystin (Tocris, catalogue no. 2267), PR-619 (Tocris, catalogue no. 4482). Where noted, protease inhibitor mixture minus EDTA (Roche, catalogue no. 11580800) was added to lysis and/or IP buffers.

Image acquisition, analysis, and quantification

Live cell imaging of neuronal spines was performed on a Nikon Eclipse Ti inverted microscope operating a Nikon A1 laser-scanning confocal system. Specimens were housed under incubation conditions throughout imaging in a gas-, temperature-, and humidity-controlled imaging chamber (Tokai Hit). Laser illumination was provided at 488 nm (air-cooled, argon ion laser at 40 milliwatt, Spectra-Physics) and 543 nm (HeNe laser at 5 milliwatt, Melles Griot). Fluorescence images were acquired with the NIS Elements AR imaging suite (Nikon, version 4.51.00) with pinhole size set to 57.5 μm (2 airy units) using a 60× oil-immersion objective (Plan Apo 60× Oil DIC N2) and 3× digital zoom. Images were captured at 1024 × 1024 pixels, with a 0.5 frames per second scan speed and 0.338-μm Z-step size. Identical settings for laser intensity and background offset were maintained between all experimental conditions. An entire dendrite emanating from one somatic branch point per neuron was fully imaged and autocompiled into a Z-stack. The Z-stacks were then reconstructed in 3D and analyzed offline using Imaris 7 software (Bitplane, version 7.7.2). Automated detection and analysis of spines was performed on single dendrites from point of initiation at the soma through 150 μm of dendrite shaft length.

ICC imaging was performed on an Olympus BX61WI upright laser-scanning confocal microscope using a 20×, 0.75 numerical aperture (NA) air (Olympus America, catalogue no. UAPO340) or 60×, 1.42 NA oil-immersion objective (Olympus America, catalogue no. PLAPON-60×) at 1024 × 1024 pixels image size and 10 μs pixel dwell time. Identical settings for gain, laser intensity, background offset, and pinhole size were maintained between all experimental conditions. Fluorescence images were then analyzed offline with the FIJI imaging suite, including the JACoP plugin (91).

PLA experiments were imaged on an Olympus IX-81 inverted spinning-disc confocal microscope using an ApoN 60×, 1.49 NA oil-immersion objective (Olympus America, catalogue no. APON 60XOTIRF) in wide-field (disc-out) configuration. Illumination was provided by a 300-watt xenon arc lamp (Sutter Instrument, LB-LS/30) coupled to an electronically shuttered liquid light guide for controlled transmission of light to the microscope optics. Images were captured with an ImagEM EM-CCD camera (catalogue no. C9100-13, Hammamtsu City, Shizuoka, Japan) with 16 μm pixel size using Metamorph image acquisition software (software version no. 7.7.1.0, Molecular Devices, Sunnyvale, CA). The following optical filter-sets were used for DAPI, mCherry, and GFP fluorophores, respectively: excitation 405/25, 472/30, 416/25, and emission 450/30, 520/35, 464/23.

Immunocytochemistry and proximity ligation assay

ICC was performed on cultured hippocampal neurons adhered to the center wells of glass-bottomed 35-mm dishes precoated with poly-D-lysine (catalogue no. P35GC-1.5-14-C, MatTek) as listed above. Cells were fixed and stained according to published protocol (92). All antibody dilutions and rinses were in PBS plus 3% BSA. Primary antibodies were added at indicated dilutions for 1 h, followed by rinses (five times, 5 min each) and addition of secondary antibodies for 45 min, followed by rinses as above, and stored in Vectashield with DAPI (catalogue no. H-1200, Vector Labs, Burlingame, CA) at 4 °C prior to imaging. PLA reactions were performed in the exact fashion as ICC procedures through primary antibody incubation. Next, anti-rabbit PLA$^+$ (catalogue no. DUO92002) and anti-mouse

PLA⁻ (catalogue no. DUO92004) probes (Sigma-Aldrich) were added for 45 min. at 37 °C, followed by rinses (three times, 5 min each, in PBS containing 0.2% BSA, 0.1% Triton X-100). Next, ligation and amplification solutions (kit catalogue no. DUO92007) were sequentially added for 30 and 100 min, respectively, with rinses as above between and prior to imaging.

Immunoprecipitation of endogenous Tomosyn-1 and HRD1 from hippocampal neuronal culture

Immunoprecipitation of endogenous protein from cultured hippocampal neurons was performed using either the Tomo-1–specific or HRD1 antibodies noted above by prebinding 2 μg antibody to 50 μl protein A magnetic DynaBead slurry (Pierce, catalogue no. 88845) per 35-mm dish in 100 mM sodium phosphate buffer (pH 8.0) containing (mM): 75 Na_2HPO_4 and 25 NaH_2PO_4. Cultures were lysed and collected in nondenaturing lysis buffer (pH 7.5) containing (mM): 50 NaCl, 25 Tris, 2 $MgCl_2$, 1 $CaCl_2$, 0.5% Nonidet P-40, and two times recommended concentration of complete EDTA-free protease inhibitor mixture. Samples were then equalized for total protein concentration (1–3 μg/μl) and sample volume (100–300 μl) prior to incubation with the conjugated beads for 1 h at 4 °C. The samples were then rinsed in lysis buffer and boiled in 1× SDS sample buffer for 5 min before being loaded for PAGE and Western blotting.

In vitro ubiquitination assay

The Gateway rat m–Tomosyn-1 construct noted above was used to express Tomo-1 in HEK293T to encourage proper post-translational modification and 3D protein structure prior to experimental procedures. Cells were seeded at 50% confluence from liquid nitrogen stocks in 10-cm cell culture dishes for ~16 h and serum-starved in 10 ml Opti-MEM (Gibco catalogue no. 31985) for 1 h prior to transfection. Transfection occurred using 25 μg plasmid DNA and 25 μl Lipofectamine 2000 (Invitrogen, catalogue no. 1166809) in 10 ml Opti-MEM, per dish, for 5 h under standard incubator conditions before standard HEK cell medium replacement. 48–72 h following transfection the cells were lysed under nondenaturing conditions in lysis buffer containing (mM): 100 Tris, 100 KCl, 0.2 EDTA, 1.5 $MgCl_2$, 0.01 pepstatin-A (Sigma, catalogue no. P5318) and protease inhibitor mixture minus EDTA (Roche) at two times recommended concentration. Lysates were then subjected to three freeze-thaw cycles using liquid nitrogen and centrifuged at 3000 × *g* for 10 min for denucleation. Nonidet P-40 was added to the lysate supernatants to a final concentration of 1% v/v. Lysates were then incubated with streptavidin-agarose beads (Invitrogen, catalogue no. S951) for 3 h at 4 °C to purify the biotinylated epitope-tagged m–Tomo-1 fusion construct. Final purity and protein concentration were quantified using a serial dilution *versus* BSA standard on a Coomassie Blue–stained SDS-PAGE gel.

For use in ubiquitin reactions, 2 μg purified Tomosyn-1 bound to the streptavidin-agarose beads were suspended in assay buffer containing the following (mM): 100 Tris, 10 $MgCl_2$, and 0.2 DTT (Invitrogen, catalogue no. 15508-013) and subjected to the following reaction conditions at 37 °C for 45 min with mixing (E3Lite Ubiquitin Ligase Kit, catalogue no. UC101, LifeSensors, Malvern, PA): 20 μg/ml wildtype human ubiquitin (catalogue no. SI201), 10 nM UBE1 (catalogue no. UB101), 100 nM UBE2D2 (catalogue no. UB207H), 16–250 nM HRD1 (catalogue no. UB307), 200 μM ATP (catalogue no. A50-09-200, SignalChem, Richmond, BC, Canada). Negative control experiments were run exactly as described above, with substitution of the E2 UBE2D2 with UBE2G2 (catalogue no. UB227) or the E3 HRD1 with CHIP/STUB1 (catalogue no. UB309).

RNA interference and lentiviral construct generation for targeting HRD1 and Tomo-1

Lentiviral vectors encoding a short hairpin RNAi (shRNA) for targeted knockdown of rat HRD1 were created in the pGFP-C-shLenti and pRFP-CB-shLenti expression vectors (Origene, Rockville, MD, catalogue nos. TL704173 and TR30032) which independently encode (via U6 promoter) the following shRNA sequences, respectively: TGGTTGGCTGAAGACCGTGTGGACTTTAT, TTGTCAGCCACGCTTATCACAGCATCCTG. Nontargeted scrambled shRNA sequences (shSCR), CAGGAACGCATAGACGCATGA, in the same lentiviral vectors were used for control experiments. Targeted knockdown of all Tomo-1 isoforms was accomplished using the same vector with the following custom shRNA sequence inserted: ACTGCTTCAGCCAGTGATTGTGTCTCCAA.

All shRNA constructs were packaged and produced at the University of Michigan Vector Core (Ann Arbor, MI). Briefly, HEK293T cells were Lipofectamine-transfected with vectors encoding REV, MDL, pvSVG, and each lentiviral plasmid-containing expression construct. At 42 h post-transfection, the virion-containing medium was collected, filtered through a 0.45-μm filter to remove cell debris, and ultra-centrifuged at 42,152 × *g* at 4 °C for 2 h. The supernatant was then discarded and the viral pellet gently resuspended in 10 ml NBActiv4 neuronal culture medium (to ~ 1×10^7 multiplicity of infection per milliliter). 500-μl aliquots were quickly frozen and stored at −80 °C. Neuronal cultures were treated with a 1:5 (HRD1 knockdown) or 1:10 (Tomo-1 knockdown) dilution of virus at 10–18 DIV and allowed to express for 4–7 days before experimentation.

Western blotting

SDS-PAGE gels were wet-transferred onto nitrocellulose membranes at 10 V for 1.2 h and blocked in non-mammalian Odyssey blocking buffer (LI-COR Biosciences, catalogue no. 927-40000). Blocking, primary antibody, and secondary antibody incubations were all performed for 1 h at room temperature and were rinsed three times for 5 min each in PBS plus 0.1% Tween-20 (PBST) between incubations. All primary antibodies were used at a 1:1,000 dilution in PBST for Western blotting, except for the following: anti-β-actin (AC74) 1:8000, anti-GFP (C163) 1:8000, and anti-ubiquitin (FK2) 1:250. All secondary antibodies were used at a 1:15,000 dilution in PBST. Western blot images were collected with an Odyssey CLx Infrared Imaging System (LI-COR model no. 9120) at 84 μm resolution in high-quality mode and within the linear range of exposure. Fluorescence density was quantified with the open-source ImageJ software including the FIJI imaging suite (93) and the gel analyzer plugin.

YFP Tomo-1 protein expression and purification

Mouse m–Tomosyn-1 (NCBI accession number NP_001074813.2) cloned into the pLenti-hSyn-eYFP backbone (22) was provided by Dr. Uri Ashery (Tel Aviv University) and used for efficient transduction and expression in cultured hippocampal neurons, as well as for immunoprecipitation following *in vivo* ubiquitination experiments. Immunoprecipitation of YFP Tomosyn proteins was performed using GFP Trap magnetic beads (catalogue no. gtma20, ChromoTek, Planegg, Germany). Cells were lysed in buffer containing: 150 mM NaCl, 50 mM Tris, 1% Nonidet P-40, 10 μM PR-619, and 2× recommended concentration of protease inhibitor mixture. Lysates were centrifuged at 10,000 × *g* and supernatants assayed using the Bradford method for total protein quantification. Total protein and volume equalizations were performed on all samples prior to incubation with the anti-GFP beads for 90 min at 4 °C to purify the YFP Tomosyn fusion construct. The samples were then rinsed in lysis buffer and boiled in 1.5× LDS sample buffer plus reducing agent (Invitrogen, catalogue nos. B0007, B0009) for 10 min before being loaded for PAGE and Western blotting.

Statistical analyses

All statistical analyses were performed with Prism 6 (version 6.0f, GraphPad Software, La Jolla, CA). Where indicated, two-tailed *t*-tests or analysis of variance (ANOVA) were used for comparisons of population means. Post hoc *t*-tests were used for multiple comparisons between specific groups. Cumulative frequency distributions were compared using a Kolmogorov-Smirnov test. Sample means throughout are presented ± S.E., with significance thresholds set to #, $p < 0.1$; *, $p < 0.05$; **, $p < 0.01$ for all tests.

Use of biological replicates

Each experiment performed in the current study used unique and independent samples (n = culture dishes for protein level biochemistry, reactions for *in vitro* ubiquitination assays, single dendrites of individual neurons for spine analysis, neurons for ICC imaging) including paired controls where noted. Significant results were determined from at least three independent neuronal preparations.

Author contributions—E. L. S. and J. J. S. conceived the study. J. J. S. and E. L. S. designed the experiments and wrote the paper. J. J. S. designed, performed, and analyzed the experiments. V. A. C. assisted in acquiring ICC fluorescence microscopy images. E. L. S., J. S., and J. J. S. designed, and J. S. and J. J. S. performed and analyzed the spine imaging experiments. All authors reviewed the results and approved a final version of the manuscript.

Acknowledgments—We thank Drs. Michael Sutton, Alan Attie, and Uri Ashery for valuable research discussion. We also thank Dr. Christina Whiteus for helpful comments on the manuscript. This research made use of the following University of Michigan core facilities: Vector, DNA Sequencing, Microscopy and Image Analysis.

References

1. Rosenberg, T., Gal-Ben-Ari, S., Dieterich, D. C., Kreutz, M. R., Ziv, N. E., Gundelfinger, E. D., and Rosenblum, K. (2014) The roles of protein expression in synaptic plasticity and memory consolidation. *Front. Mol. Neurosci.* **7,** 86 CrossRef Medline
2. Sutton, M. A., and Schuman, E. M. (2006) Dendritic protein synthesis, synaptic plasticity, and memory. *Cell* **127,** 49–58 CrossRef Medline
3. Hegde, A. N., Goldberg, A. L., and Schwartz, J. H. (1993) Regulatory subunits of cAMP-dependent protein kinases are degraded after conjugation to ubiquitin: A molecular mechanism underlying long-term synaptic plasticity. *Proc. Natl. Acad. Sci. U.S.A.* **90,** 7436–7440 CrossRef Medline
4. Hegde, A. N. (2017) Proteolysis, synaptic plasticity and memory. *Neurobiol. Learn. Mem.* **138,** 98–110 CrossRef Medline
5. Alvarez-Castelao, B., and Schuman, E. M. (2015) The regulation of synaptic protein turnover. *J. Biol. Chem.* **290,** 28623–28630 CrossRef Medline
6. Pak, D. T. S., and Sheng, M. (2003) Targeted protein degradation and synapse remodeling by an inducible protein kinase. *Science* **302,** 1368–1373 CrossRef Medline
7. Patrick, G. N. (2006) Synapse formation and plasticity: Recent insights from the perspective of the ubiquitin proteasome system. *Curr. Opin. Neurobiol.* **16,** 90–94 CrossRef Medline
8. Waites, C. L., Leal-Ortiz, S. A., Okerlund, N., Dalke, H., Fejtova, A., Altrock, W. D., Gundelfinger, E. D., and Garner, C. C. (2013) Bassoon and Piccolo maintain synapse integrity by regulating protein ubiquitination and degradation. *EMBO J.* **32,** 954–969 CrossRef Medline
9. Jiang, X., Litkowski, P. E., Taylor, A. A., Lin, Y., Snider, B. J., and Moulder, K. L. (2010) A role for the ubiquitin-proteasome system in activity-dependent presynaptic silencing. *J. Neurosci.* **30,** 1798–1809 CrossRef Medline
10. Zhang, Q., Li, Y., Zhang, L., Yang, N., Meng, J., Zuo, P., Zhang, Y., Chen, J., Wang, L., Gao, X., and Zhu, D. (2013) E3 ubiquitin ligase RNF13 involves spatial learning and assembly of the SNARE complex. *Cell. Mol. Life Sci.* **70,** 153–165 CrossRef Medline
11. Ehlers, M. D. (2003) Activity level controls postsynaptic composition and signaling via the ubiquitin-proteasome system. *Nat. Neurosci.* **6,** 231–242 CrossRef Medline
12. Schwarz, L. A., and Patrick, G. N. (2012) Ubiquitin-dependent endocytosis, trafficking and turnover of neuronal membrane proteins. *Mol. Cell. Neurosci.* **49,** 387–393 CrossRef Medline
13. Colledge, M., Snyder, E. M., Crozier, R. A., Soderling, J. A., Jin, Y., Langeberg, L. K., Lu, H., Bear, M. F., and Scott, J. D. (2003) Ubiquitination regulates PSD-95 degradation and AMPA receptor surface expression. *Neuron* **40,** 595–607 CrossRef Medline
14. Bingol, B., and Schuman, E. M. (2006) Activity-dependent dynamics and sequestration of proteasomes in dendritic spines. *Nature* **441,** 1144–1148 CrossRef Medline
15. Hamilton, A. M., Oh, W. C., Vega-Ramirez, H., Stein, I. S., Hell, J. W., Patrick, G. N., and Zito, K. (2012) Activity-dependent growth of new dendritic spines is regulated by the proteasome. *Neuron* **74,** 1023–1030 CrossRef Medline
16. Huang, J., Ikeuchi, Y., Malumbres, M., and Bonni, A. (2015) A Cdh1-APC/FMRP ubiquitin signaling link drives mGluR-dependent synaptic plasticity in the mammalian brain. *Neuron* **86,** 726–739 CrossRef Medline
17. Ashery, U., Bielopolski, N., Barak, B., and Yizhar, O. (2009) Friends and foes in synaptic transmission: The role of tomosyn in vesicle priming. *Trends Neurosci.* **32,** 275–282 CrossRef Medline
18. Lehman, K., Rossi, G., Adamo, J. E., and Brennwald, P. (1999) Yeast homologues of tomosyn and lethal giant larvae function in exocytosis and are associated with the plasma membrane SNARE, Sec9. *J. Cell Biol.* **146,** 125–140 Medline
19. Sakisaka, T., Yamamoto, Y., Mochida, S., Nakamura, M., Nishikawa, K., Ishizaki, H., Okamoto-Tanaka, M., Miyoshi, J., Fujiyoshi, Y., Manabe, T., and Takai, Y. (2008) Dual inhibition of SNARE complex formation by tomosyn ensures controlled neurotransmitter release. *J. Cell Biol.* **183,** 323–337 CrossRef Medline
20. Bielopolski, N., Lam, A. D., Bar-On, D., Sauer, M., Stuenkel, E. L., and Ashery, U. (2014) Differential interaction of Tomosyn with Syntaxin and SNAP25 depends on domains in the WD40-propeller core and determines its inhibitory activity. *J. Biol. Chem.* **289,** 17087–17099 CrossRef Medline
21. Chen, K., Richlitzki, A., Featherstone, D. E., Schwärzel, M., and Richmond, J. E. (2011) Tomosyn-dependent regulation of synaptic transmission is

required for a late phase of associative odor memory. *Proc. Natl. Acad. Sci. U.S.A.* **108,** 18482–18487 CrossRef Medline

22. Barak, B., Okun, E., Ben-Simon, Y., Lavi, A., Shapira, R., Madar, R., Wang, Y., Norman, E., Sheinin, A., Pita, M. A., Yizhar, O., Mughal, M. R., Stuenkel, E., van Praag, H., Mattson, M. P., and Ashery, U. (2013) Neuron-specific expression of tomosyn1 in the mouse hippocampal dentate gyrus impairs spatial learning and memory. *Neuromolecular Med.* **15,** 351–363 CrossRef Medline
23. Ben-Simon, Y., Rodenas-Ruano, A., Alviña, K., Lam, A. D., Stuenkel, E. L., Castillo, P. E., and Ashery, U. (2015) A combined optogenetic-knockdown strategy reveals a major role of Tomosyn in mossy fiber synaptic plasticity. *Cell Rep.* **12,** 396–404 CrossRef Medline
24. Cheviet, S., Bezzi, P., Ivarsson, R., Renström, E., Viertl, D., Kasas, S., Catsicas, S., and Regazzi, R. (2006) Tomosyn-1 is involved in a post-docking event required for pancreatic beta-cell exocytosis. *J. Cell Sci.* **119,** 2912–2920 CrossRef Medline
25. Zhang, W., Lilja, L., Mandic, S. A., Gromada, J., Smidt, K., Janson, J., Takai, Y., Bark, C., Berggren, P.-O., and Meister, B. (2006) Tomosyn is expressed in beta-cells and negatively regulates insulin exocytosis. *Diabetes* **55,** 574–581 CrossRef Medline
26. Fujita, Y., Shirataki, H., Sakisaka, T., Asakura, T., Ohya, T., Kotani, H., Yokoyama, S., Nishioka, H., Matsuura, Y., Mizoguchi, A., Scheller, R. H., and Takai, Y. (1998) Tomosyn: A syntaxin-1-binding protein that forms a novel complex in the neurotransmitter release process. *Neuron* **20,** 905–915 CrossRef Medline
27. McEwen, J. M., Madison, J. M., Dybbs, M., and Kaplan, J. M. (2006) Antagonistic regulation of synaptic vesicle priming by Tomosyn and UNC-13. *Neuron* **51,** 303–315 CrossRef Medline
28. Takamori, S., Holt, M., Stenius, K., Lemke, E. A., Grønborg, M., Riedel, D., Urlaub, H., Schenck, S., Brügger, B., Ringler, P., Müller, S. A., Rammner, B., Gräter, F., Hub, J. S., De Groot, B. L., *et al.* (2006) Molecular anatomy of a trafficking organelle. *Cell* **127,** 831–846 CrossRef Medline
29. Sakisaka, T., Baba, T., Tanaka, S., Izumi, G., Yasumi, M., and Takai, Y. (2004) Regulation of SNAREs by tomosyn and ROCK: Implication in extension and retraction of neurites. *J. Cell Biol.* **166,** 17–25 CrossRef Medline
30. Cazares, V. A., Njus, M. M., Manly, A., Saldate, J. J., Subramani, A., Ben-Simon, Y., Sutton, M. A., Ashery, U., and Stuenkel, E. L. (2016) Dynamic partitioning of synaptic vesicle pools by the SNARE-binding protein Tomosyn. *J. Neurosci.* **36,** 11208–11222 CrossRef Medline
31. Watson, K., Rossi, G., Temple, B., and Brennwald, P. (2015) Structural basis for recognition of the Sec4 Rab GTPase by its effector, the Lgl/tomosyn homologue, Sro7. *Mol. Biol. Cell* **26,** 3289–3300 CrossRef Medline
32. Burdina, A. O., Klosterman, S. M., Shtessel, L., Ahmed, S., and Richmond, J. E. (2011) *In vivo* analysis of conserved *C. elegans* tomosyn domains. *PLoS One* **6,** e26185–e26188 CrossRef Medline
33. Pobbati, A. V., Razeto, A., Böddener, M., Becker, S., and Fasshauer, D. (2004) Structural basis for the inhibitory role of tomosyn in exocytosis. *J. Biol. Chem.* **279,** 47192–47200 CrossRef Medline
34. Yizhar, O., Lipstein, N., Gladycheva, S. E., Matti, U., Ernst, S. A., Rettig, J., Stuenkel, E. L., and Ashery, U. (2007) Multiple functional domains are involved in tomosyn regulation of exocytosis. *J. Neurochem.* **103,** 604–616 CrossRef Medline
35. Yamamoto, Y., Mochida, S., Miyazaki, N., Kawai, K., Fujikura, K., Kurooka, T., Iwasaki, K., and Sakisaka, T. (2010) Tomosyn inhibits synaptotagmin-1-mediated step of Ca^{2+}-dependent neurotransmitter release through its N-terminal WD40 repeats. *J. Biol. Chem.* **285,** 40943–40955 CrossRef Medline
36. Baba, T., Sakisaka, T., Mochida, S., and Takai, Y. (2005) PKA-catalyzed phosphorylation of tomosyn and its implication in Ca^{2+}-dependent exocytosis of neurotransmitter. *J. Cell Biol.* **170,** 1113–1125 CrossRef Medline
37. Hattendorf, D. A., Andreeva, A., Gangar, A., Brennwald, P. J., and Weis, W. I. (2007) Structure of the yeast polarity protein Sro7 reveals a SNARE regulatory mechanism. *Nature* **446,** 567–571 CrossRef Medline
38. Rossi, G., Watson, K., Demonch, M., Temple, B., and Brennwald, P. (2015) *In vitro* reconstitution of Rab-dependent vesicle clustering by the yeast lethal giant larvae/tomosyn homolog, Sro7. *J. Biol. Chem.* **290,** 612–624 CrossRef Medline
39. Hu, Z., Hom, S., Kudze, T., Tong, X.-J., Choi, S., Aramuni, G., Zhang, W., and Kaplan, J. M. (2012) Neurexin and neuroligin mediate retrograde synaptic inhibition in *C. elegans*. *Science* **337,** 980–984 CrossRef Medline
40. Williams, A. L., Bielopolski, N., Meroz, D., Lam, A. D., Passmore, D. R., Ben-Tal, N., Ernst, S. A., Ashery, U., and Stuenkel, E. L. (2011) Structural and functional analysis of tomosyn identifies domains important in exocytotic regulation. *J. Biol. Chem.* **286,** 14542–14553 CrossRef Medline
41. Geerts, C. J., Jacobsen, L., van de Bospoort, R., Verhage, M., and Groffen, A. J. A. (2014) Tomosyn interacts with the SUMO E3 ligase PIASγ. *PLoS One* **9,** e91697–e91698 CrossRef Medline
42. Barak, B., Williams, A., Bielopolski, N., Gottfried, I., Okun, E., Brown, M. A., Matti, U., Rettig, J., Stuenkel, E. L., and Ashery, U. (2010) Tomosyn expression pattern in the mouse hippocampus suggests both presynaptic and postsynaptic functions. *Front. Neuroanat.* **4,** 149 CrossRef Medline
43. Bhatnagar, S., Soni, M. S., Wrighton, L. S., Hebert, A. S., Zhou, A. S., Paul, P. K., Gregg, T., Rabaglia, M. E., Keller, M. P., Coon, J. J., and Attie, A. D. (2014) Phosphorylation and degradation of tomosyn-2 de-represses insulin secretion. *J. Biol. Chem.* **289,** 25276–25286 CrossRef Medline
44. Davis, L. K., Meyer, K. J., Rudd, D. S., Librant, A. L., Epping, E. A., Sheffield, V. C., and Wassink, T. H. (2009) Novel copy number variants in children with autism and additional developmental anomalies. *J. Neurodev. Disord.* **1,** 292–301 CrossRef Medline
45. Bolte, E. R. (2003) The role of cellular secretion in autism spectrum disorders: A unifying hypothesis. *Med. Hypotheses* **60,** 119–122 CrossRef Medline
46. Lehman, N. L. (2009) The ubiquitin proteasome system in neuropathology. *Acta Neuropathol.* **118,** 329–347 CrossRef Medline
47. Sharma, M., Burré, J., and Südhof, T. C. (2012) Proteasome inhibition alleviates SNARE-dependent neurodegeneration. *Sci. Transl. Med.* **4,** 147ra113 CrossRef Medline
48. Hegde, A. N., Haynes, K. A., Bach, S. V., and Beckelman, B. C. (2014) Local ubiquitin-proteasome-mediated proteolysis and long-term synaptic plasticity. *Front. Mol. Neurosci.* **7,** 96 CrossRef Medline
49. Shin, J.-H., Ko, H. S., Kang, H., Lee, Y., Lee, Y.-I., Pletinkova, O., Troconso, J. C., Dawson, V. L., and Dawson, T. M. (2011) PARIS (ZNF746) repression of PGC-1α contributes to neurodegeneration in Parkinson's disease. *Cell* **144,** 689–702 CrossRef Medline
50. Garcia-Reitböck, P., Anichtchik, O., Bellucci, A., Iovino, M., Ballini, C., Fineberg, E., Ghetti, B., Della Corte, L., Spano, P., Tofaris, G. K., Goedert, M., and Spillantini, M. G. (2010) SNARE protein redistribution and synaptic failure in a transgenic mouse model of Parkinson's disease. *Brain* **133,** 2032–2044 CrossRef Medline
51. Lin, Y.-C., Frei, J. A., Kilander, M. B. C., Shen, W., and Blatt, G. J. (2016) A subset of autism-associated genes regulate the structural stability of neurons. *Front. Cell Neurosci.* **10,** 805–835 CrossRef Medline
52. Nadav, E., Shmueli, A., Barr, H., Gonen, H., Ciechanover, A., and Reiss, Y. (2003) A novel mammalian endoplasmic reticulum ubiquitin ligase homologous to the yeast Hrd1. *Biochem. Biophys. Res. Commun.* **303,** 91–97 CrossRef Medline
53. Kaneko, M., Ishiguro, M., Niinuma, Y., Uesugi, M., and Nomura, Y. (2002) Human HRD1 protects against ER stress-induced apoptosis through ER-associated degradation. *FEBS Letters* **532,** 147–152 CrossRef Medline
54. Gauss, R., Jarosch, E., Sommer, T., and Hirsch, C. (2006) A complex of Yos9p and the HRD ligase integrates endoplasmic reticulum quality control into the degradation machinery. *Nat. Cell Biol.* **8,** 849–854 CrossRef Medline
55. Omura, T., Kaneko, M., Tabei, N., Okuma, Y., and Nomura, Y. (2008) Immunohistochemical localization of a ubiquitin ligase HRD1 in murine brain. *J. Neurosci. Res.* **86,** 1577–1587 CrossRef Medline
56. Groffen, A. J. A., Jacobsen, L., Schut, D., and Verhage, M. (2005) Two distinct genes drive expression of seven tomosyn isoforms in the mammalian brain, sharing a conserved structure with a unique variable domain. *J. Neurochem.* **92,** 554–568 CrossRef Medline
57. Ramírez, O. A., and Couve, A. (2011) The endoplasmic reticulum and protein trafficking in dendrites and axons. *Trends Cell Biol.* **21,** 219–227 CrossRef Medline

58. Murakami, T., Hino, S. I., Saito, A., and Imaizumi, K. (2007) Endoplasmic reticulum stress response in dendrites of cultured primary neurons. *Neuroscience* **146,** 1–8 CrossRef Medline
59. Kawada, K., Iekumo, T., Saito, R., Kaneko, M., Mimori, S., Nomura, Y., and Okuma, Y. (2014) Aberrant neuronal differentiation and inhibition of dendrite outgrowth resulting from endoplasmic reticulum stress. *J. Neurosci. Res.* **92,** 1122–1133 CrossRef Medline
60. Kienle, N., Kloepper, T. H., and Fasshauer, D. (2009) Phylogeny of the SNARE vesicle fusion machinery yields insights into the conservation of the secretory pathway in fungi. *BMC Evol. Biol.* **9,** 19 CrossRef Medline
61. Petrovski, S., Wang, Q., Heinzen, E. L., Allen, A. S., and Goldstein, D. B. (2013) Genic intolerance to functional variation and the interpretation of personal genomes. *PLoS Genet.* **9,** e1003709 CrossRef Medline
62. Gladycheva, S. E., Lam, A. D., Liu, J., D'Andrea-Merrins, M., Yizhar, O., Lentz, S. I., Ashery, U., Ernst, S. A., and Stuenkel, E. L. (2007) Receptor-mediated regulation of tomosyn-syntaxin 1A interactions in bovine adrenal chromaffin cells. *J. Biol. Chem.* **282,** 22887–22899 CrossRef Medline
63. Hatsuzawa, K., Lang, T., Fasshauer, D., Bruns, D., and Jahn, R. (2003) The R-SNARE motif of tomosyn forms SNARE core complexes with syntaxin 1 and SNAP-25 and down-regulates exocytosis. *J. Biol. Chem.* **278,** 31159–31166 CrossRef Medline
64. Nagano, K., Takeuchi, H., Gao, J., Mori, Y., Otani, T., Wang, D., and Hirata, M. (2015) Tomosyn is a novel Akt substrate mediating insulin-dependent GLUT4 exocytosis. *Int. J. Biochem. Cell Biol.* **62,** 62–71 CrossRef Medline
65. Gracheva, E. O., Burdina, A. O., Holgado, A. M., Berthelot-Grosjean, M., Ackley, B. D., Hadwiger, G., Nonet, M. L., Weimer, R. M., and Richmond, J. E. (2006) Tomosyn inhibits synaptic vesicle priming in *Caenorhabditis elegans*. *PLoS Biol.* **4,** e261 CrossRef Medline
66. Yizhar, O., Matti, U., Melamed, R., Hagalili, Y., Bruns, D., Rettig, J., and Ashery, U. (2004) Tomosyn inhibits priming of large dense-core vesicles in a calcium-dependent manner. *Proc. Natl. Acad. Sci. U.S.A.* **101,** 2578–2583 CrossRef Medline
67. Kagami, M., Toh-e, A, Matsui, Y. (1998) Sro7p, a *Saccharomyces cerevisiae* counterpart of the tumor suppressor l(2)gl protein, is related to myosins in function. *Genetics* **149,** 1717–1727 Medline
68. Gangar, A., Rossi, G., Andreeva, A., Hales, R., and Brennwald, P. (2005) Structurally conserved interaction of Lgl family with SNAREs is critical to their cellular function. *Curr. Biol.* **15,** 1136–1142 CrossRef Medline
69. Rossi, G., and Brennwald, P. (2011) Yeast homologues of lethal giant larvae and type V myosin cooperate in the regulation of Rab-dependent vesicle clustering and polarized exocytosis. *Mol. Biol. Cell* **22,** 842–857 CrossRef Medline
70. Cohen, L. D., Zuchman, R., Sorokina, O., Müller, A., Dieterich, D. C., Armstrong, J. D., Ziv, T., and Ziv, N. E. (2013) Metabolic turnover of synaptic proteins: Kinetics, interdependencies and implications for synaptic maintenance. *PLoS One* **8,** e63191 CrossRef Medline
71. Nalavadi, V. C., Muddashetty, R. S., Gross, C., and Bassell, G. J. (2012) Dephosphorylation-induced ubiquitination and degradation of FMRP in dendrites: A role in immediate early mGluR-stimulated translation. *J. Neurosci.* **32,** 2582–2587 CrossRef Medline
72. Pavlopoulos, E., Trifilieff, P., Chevaleyre, V., Fioriti, L., Zairis, S., Pagano, A., Malleret, G., and Kandel, E. R. (2011) Neuralized1 activates CPEB3: A function for nonproteolytic ubiquitin in synaptic plasticity and memory storage. *Cell* **147,** 1369–1383 CrossRef Medline
73. Hamilton, A. M., and Zito, K. (2013) Breaking it down: The ubiquitin proteasome system in neuronal morphogenesis. *Neural Plast.* **2013,** 1–10 CrossRef Medline
74. Mabb, A. M., and Ehlers, M. D. (2010) Ubiquitination in postsynaptic function and plasticity. *Annu. Rev. Cell Dev. Biol.* **26,** 179–210 CrossRef Medline
75. Tsai, N.-P. (2014) Ubiquitin proteasome system-mediated degradation of synaptic proteins: An update from the postsynaptic side. *Mol. Cell Res.* **1843,** 2838–2842 CrossRef Medline
76. Dindot, S. V., Antalffy, B. A., Bhattacharjee, M. B., and Beaudet, A. L. (2008) The Angelman syndrome ubiquitin ligase localizes to the synapse and nucleus, and maternal deficiency results in abnormal dendritic spine morphology. *Hum. Mol. Genet.* **17,** 111–118 CrossRef Medline
77. Kim, H., Kunz, P. A., Mooney, R., Philpot, B. D., and Smith, S. L. (2016) Maternal loss of Ube3a impairs experience-driven dendritic spine maintenance in the developing visual cortex. *J. Neurosci.* **36,** 4888–4894 CrossRef Medline
78. Guntupalli, S., Jang, S. E., Zhu, T., Huganir, R. L., Widagdo, J., and Anggono, V. (2017) GluA1 subunit ubiquitination mediates amyloid-β-induced loss of surface α-amino-3-hydroxy-5-methyl-4-isoxazolepropionic acid (AMPA) receptors. *J. Biol. Chem.* **292,** 8186–8194 CrossRef Medline
79. Schreiber, J., Végh, M. J., Dawitz, J., Kroon, T., Loos, M., Labonté, D., Li, K. W., Van Nierop, P., Van Diepen, M. T., De Zeeuw, C. I., Kneussel, M., Meredith, R. M., Smit, A. B., and Van Kesteren, R. E. (2015) Ubiquitin ligase TRIM3 controls hippocampal plasticity and learning by regulating synaptic γ-actin levels. *J. Cell Biol.* **211,** 569–586 CrossRef Medline
80. Hung, A. Y., Sung, C. C., Brito, I. L., and Sheng, M. (2010) Degradation of postsynaptic scaffold GKAP and regulation of dendritic spine morphology by the TRIM3 ubiquitin ligase in rat hippocampal neurons. *PLoS ONE* **5,** e9842-11 CrossRef Medline
81. Bianchetta, M. J., Lam, T. T., Jones, S. N., and Morabito, M. A. (2011) Cyclin-dependent kinase 5 regulates PSD-95 ubiquitination in neurons. *J. Neurosci.* **31,** 12029–12035 CrossRef Medline
82. Lussier, M. P., Herring, B. E., Nasu-Nishimura, Y., Neutzner, A., Karbowski, M., Youle, R. J., Nicoll, R. A., and Roche, K. W. (2012) Ubiquitin ligase RNF167 regulates AMPA receptor-mediated synaptic transmission. *Proc. Natl. Acad. Sci. U.S.A.* **109,** 19426–19431 CrossRef Medline
83. Greer, P. L., Hanayama, R., Bloodgood, B. L., Mardinly, A. R., Lipton, D. M., Flavell, S. W., Kim, T.-K., Griffith, E. C., Waldon, Z., Maehr, R., Ploegh, H. L., Chowdhury, S., Worley, P. F., Steen, J., and Greenberg, M. E. (2010) The Angelman syndrome protein Ube3A regulates synapse development by ubiquitinating arc. *Cell* **140,** 704–716 CrossRef Medline
84. Mabb, A. M., Je, H. S., Wall, M. J., Robinson, C. G., Larsen, R. S., Qiang, Y., Corrêa, S. A. L., and Ehlers, M. D. (2014) Triad3A regulates synaptic strength by ubiquitination of arc. *Neuron* **82,** 1299–1316 CrossRef Medline
85. Yao, I., Takagi, H., Ageta, H., Kahyo, T., Sato, S., Hatanaka, K., Fukuda, Y., Chiba, T., Morone, N., Yuasa, S., Inokuchi, K., Ohtsuka, T., MacGregor, G. R., Tanaka, K., and Setou, M. (2007) SCRAPPER-dependent ubiquitination of active zone protein RIM1 regulates synaptic vesicle release. *Cell* **130,** 943–957 CrossRef Medline
86. Yang, H., Zhong, X., Ballar, P., Luo, S., Shen, Y., Rubinsztein, D. C., Monteiro, M. J., and Fang, S. (2007) Ubiquitin ligase Hrd1 enhances the degradation and suppresses the toxicity of polyglutamine-expanded huntingtin. *Exp. Cell Res.* **313,** 538–550 CrossRef Medline
87. Mao, J., Xia, Q., Liu, C., Ying, Z., Wang, H., and Wang, G. (2017) A critical role of Hrd1 in the regulation of optineurin degradation and aggresome formation. *Hum. Mol. Genet.* **26,** 1877–1889 CrossRef Medline
88. Ying, H., Yue, B. Y. J. T. (2012) Cellular and molecular biology of optineurin. *Int. Rev. Cell Mol. Biol.* **294,** 223–258 CrossRef Medline
89. Zhang, P., Fu, W.-Y., Fu, A. K. Y., and Ip, N. Y. (2015) S-nitrosylation-dependent proteasomal degradation restrains Cdk5 activity to regulate hippocampal synaptic strength. *Nat. Commun.* **6,** 1–11 CrossRef Medline
90. Jakawich, S. K., Nasser, H. B., Strong, M. J., McCartney, A. J., Perez, A. S., Rakesh, N., Carruthers, C. J. L., and Sutton, M. A. (2010) Local presynaptic activity gates homeostatic changes in presynaptic function driven by dendritic BDNF synthesis. *Neuron* **68,** 1143–1158 CrossRef Medline
91. Bolte, S., and Cordelières, F. P. (2006) A guided tour into subcellular colocalization analysis in light microscopy. *J. Microsc.* **224,** 213–232 CrossRef Medline
92. Glynn, M. W., and McAllister, A. K. (2006) Immunocytochemistry and quantification of protein colocalization in cultured neurons. *Nat. Protoc.* **1,** 1287–1296 CrossRef Medline
93. Schindelin, J., Arganda-Carreras, I., Frise, E., Kaynig, V., Longair, M., Pietzsch, T., Preibisch, S., Rueden, C., Saalfeld, S., Schmid, B., Tinevez, J.-Y., White, D. J., Hartenstein, V., Eliceiri, K., Tomancak, P., and Cardona, A. (2012) Fiji: An open-source platform for biological-image analysis. *Nat. Meth.* **9,** 676–682 CrossRef Medline